Acta Crystallographica Section B
Structural Science
ISSN 0108-7681

Structures of cyclic dipeptides: an X-ray and computational study of *cis*- and *trans*-*cyclo*(Pip-Phe), *cyclo*(Pro-Phe) and their *N*-methyl derivatives

Milos Budesinsky,[a]* Ivana Cisarova,[b] Jaroslav Podlaha,[b] Frans Borremans,[c] José C. Martins,[c] Michel Waroquier[d] and Ewald Pauwels[d]*

[a]Institute of Organic Chemistry and Biochemistry, Academy of Sciences of the Czech Republic, Flemingovo 2, CZ-166 10 Prague 6, Czech Republic, [b]Department of Inorganic Chemistry, Charles University, Hlavova 2040, CZ-128 40 Prague 2, Czech Republic, [c]NMR and Structure Analysis Unit, Ghent University, Krijgslaan 281 S4, B-9000 Ghent, Belgium, and [d]Center for Molecular Modeling, Ghent University, Technologiepark 903, B-9052 Zwijnaarde, Belgium

Correspondence e-mail: budesinsky@uochb.cas.cz, ewald.pauwels@ugent.be

Received 17 May 2010
Accepted 8 October 2010

The crystal structures of eight cyclodipeptides are determined, incorporating pipecolic acid or proline and phenylalanine or *N*-methyl phenylalanine. This set of structures allows the evaluation of the effects on molecular conformation and crystal packing of imino acid ring-size, relative configuration of the two amino acids, and *N*-methylation. In the non-methylated compounds, hydrogen-bonding interactions form one-dimensional motifs that dominate the packing arrangement. Three compounds have more than one symmetry-independent molecule in the asymmetric unit ($Z' > 1$), indicative of a broad and shallow molecular energy minimum. Density functional theory calculations reveal the interplay between inter- and intramolecular factors in the crystals. Only for the *N*-methylated compounds do simulations of the molecules in the isolated state succeed to reproduce the observed crystallographic conformations. Puckering of the diketopiperazine ring and the deviation from planarity of the amide bonds are not reproduced in the remaining compounds. *Cluster in vacuo* calculations with a central cyclodipeptide molecule surrounded by hydrogen-bound molecules establish that hydrogen bonding is of major importance but that other intermolecular interactions must also contribute substantially to the crystal structure. More advanced periodic calculations, incorporating the crystallographic environment to the full extent, are necessary to correctly describe all the conformational features of these cyclodipeptide crystals.

1. Introduction

Cyclic dipeptides (2,5-diketopiperazines or DKPs) represent an important class of biologically active natural compounds (Sammers, 1975). As unique and simple model systems for peptides and proteins they have been the subject of intensive research that is fundamental to many aspects of synthetic and structural peptide chemistry (Anteunis, 1978; Rajappa & Natekar, 1993; Fischer, 2003). Nowadays there are three new aspects that attract interest to DKPs:

(i) their possible use as simple heterocyclic scaffolds in combinatorial chemistry (Fischer, 2003);

(ii) the availability of computational *ab initio* methods which allow an in-depth evaluation of structural as well as spectral features for these simple models (Bouř *et al.*, 2002; Zhu *et al.*, 2006);

(iii) their role as model compounds in crystal engineering, *i.e.* the prediction of solid-state structure and the control over intermolecular forces that determine molecular packing patterns in organic crystals (MacDonald & Whitesides, 1994; Desiraju, 1995; Palacin *et al.*, 1997; Chin *et al.*, 1999).

The vast majority of experimental data on the conformation of cyclic dipeptides originate from X-ray studies on crystals or from NMR investigations in solution. The interpretation of structural features in the condensed phase is complicated, as it is the result of the interplay of intra- and intermolecular factors. At present, structures of cyclic dipeptides in the gas phase are hardly accessible experimentally. However, modern *ab initio* tools based on quantum chemistry can provide a detailed and reliable approximation of the geometry of energy-minimized single molecules. Methods based on density functional theory (DFT), in particular, are well established in this respect and accurately describe the gas-phase conformation of a particular molecule at a reasonable computational cost (Koch & Holthausen, 2001). However, as a result of the ever-increasing computer power, condensed phase simulations are also gradually becoming more common.

We are currently undertaking a full characterization of the structural features of 28 cyclodipeptides (Fig. 1) in the solid state as well as in solution using the two most powerful experimental methods (X-ray structure analysis and NMR spectroscopy) in combination with a theoretical analysis based on *ab initio* calculations. These compounds are suitable models for the evaluation of the effects of:

(i) the ring size of the cyclic imino acid,

(ii) the substitution of a CH_2 group by sulfur in the cyclic imino acid,

(iii) *N*-methylation, and

(iv) the relative configuration of amino acid residues.

The fusion with five- or six-membered rings is known to substantially alter the conformation of the DKP ring. The *N*-methylated cyclodipeptides are chosen to eliminate hydrogen bonding and to introduce steric strain with the Phe side-chain. The aromatic ring of Phe and the S atom can be involved in different types of intra- and intermolecular interactions.

We have carefully selected eight cyclodipeptides, (1*A*), (1*B*), (2*A*), (2*B*), (9*A*), (9*B*), (10*A*) and (10*B*) (shown in red in Fig. 1), to constitute a reference set. These compounds are suitably diverse to function as a reference, since they display a large variation in conformational flexibility for the factors that are currently understood to determine the conformation of cyclic dipeptides. At the same time, the set provides sufficient diversity in the type of crystal packing forces. The reference set will function as the basis for the evaluation of the effects of sulfur observed in the 20 remaining sulfur analogs (shown in black in Fig. 1). These analogs, in which a CH_2 group is substituted by sulfur at the β, γ or δ position of Pip [(3*A*)–(8*B*)] or the β or γ position of Pro [(11*A*)–(14*B*)], will be the subject of a future report.

In this work, a detailed description is given of the molecular conformation and packing in the crystal structures of the eight reference compounds and the impact of their primary structural differences (imino acid ring size, *N*-methylation and relative configuration) is documented. Furthermore, by combining the experimental X-ray data with *ab initio* calculations, we explore the interplay between intermolecular and intramolecular interactions in the packing of molecules within the crystal. By separating these interactions, we examine how they contribute to the individual molecular conformations and their deformation(s) in the asymmetric unit.

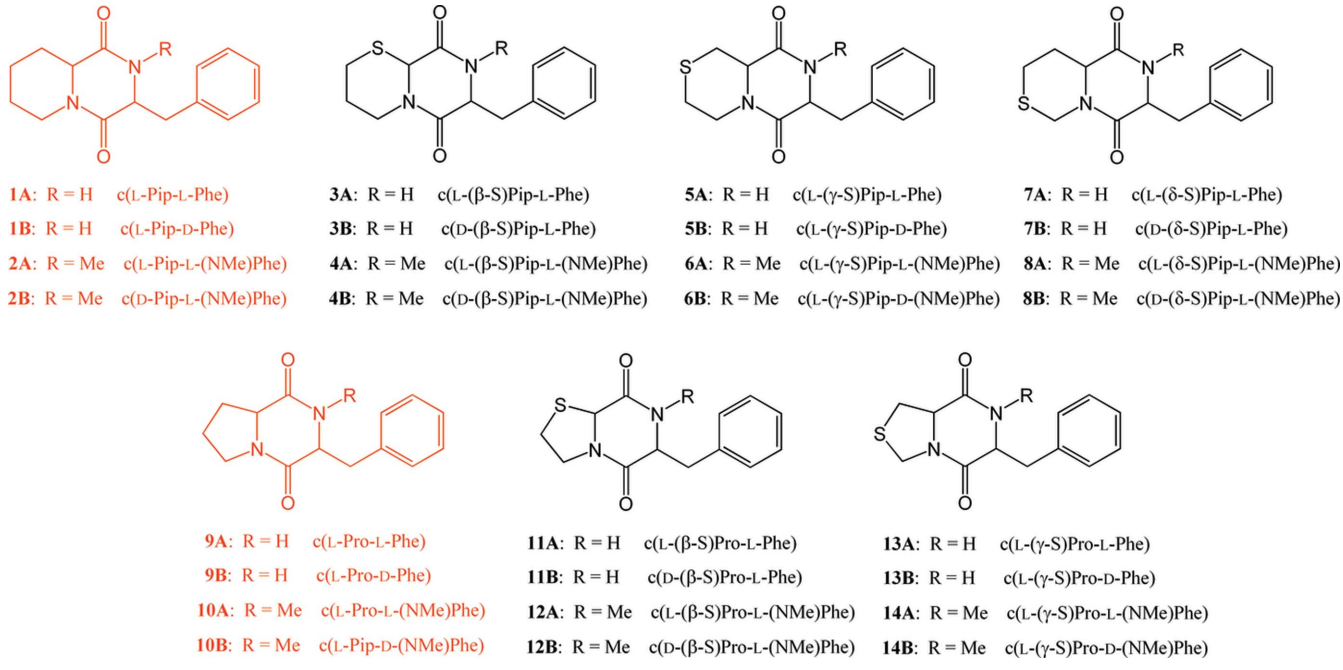

Figure 1
Structure of selected cyclodipeptides (those discussed in the text are shown in red). The *A* and *B* labels refer to the different diastereomers. Even and odd numbers refer to *N*-methylated and non-methylated compounds. This figure is in color in the electronic version of this paper.

Table 1
Experimental details on crystal structure analysis of (1*A*)–(2*B*) and (9*A*)–(10*B*).

Experiments were carried out with Mo $K\alpha$ radiation. The absolute structure was obtained using Flack (1983).

	(1*A*)	(1*B*)	(2*A*)	(2*B*)
Crystal data				
Chemical formula	$2C_{15}H_{18}N_4O_4{\cdot}H_2O$	$C_{15}H_{18}N_2O_2$	$C_{16}H_{20}N_2O_2$	$C_{16}H_{20}N_2O_2$
M_r	534.64	258.31	272.34	272.34
Crystal system, space group	Monoclinic, $P2_1$	Monoclinic, $P2_1$	Triclinic, $P1$	Orthorhombic, $P2_12_12_1$
Temperature (K)	150	150	150	150
a, b, c (Å)	8.4202 (2), 24.7788 (4), 13.4204 (3)	22.1154 (7), 6.3963 (2), 29.5771 (7)	7.4277 (2), 7.4388 (3), 13.5369 (5)	10.0530 (3), 10.8372 (2), 13.3352 (5)
α, β, γ (°)	90, 91.6730 (11), 90	90, 95.2660 (18), 90	90.176 (2), 79.737 (2), 70.800 (2)	90, 90, 90
V (Å^3)	2798.87 (10)	4166.2 (2)	693.52 (4)	1452.82 (7)
Z	4	12	2	4
Z'	2	6	2	1
μ (mm^{-1})	0.087	0.083	0.087	0.083
$F(000)$	1144	1656	292	584
Crystal size (mm)	0.25 × 0.25 × 0.30	0.20 × 0.35 × 0.35	0.25 × 0.35 × 0.50	0.20 × 0.35 × 0.35
Data collection				
Diffractometer	Nonius KappaCCD area detector	Nonius KappaCCD area detector	Nonius KappaCCD area detector	Nonius KappaCCD area detector
θ_{max} (°)	25.0	25.1	27.2	27.5
Dataset	−10: 9; −29: 27; −15: 15	−26: 26; −7: 7; −34: 35	−9: 9; −9: 9; −17: 15	−13: 13; −14: 14; −17: 17
No. of measured, independent and observed [$I > 2\sigma(I)$] reflections	31 329, 9713, 8038	64 641, 14 267, 9326	11 078, 5078, 4906	19 589, 3329, 3001
R_{int}	0.060	0.036	0.070	0.034
Refinement				
$R[F^2 > 2\sigma(F^2)]$, $wR(F^2)$, S(all data)	0.054, 0.137, 1.04	0.066, 0.144, 1.08	0.039, 0.101, 1.08	0.035, 0.084, 1.06
No. of reflections	9713	14 267	5078	3329
No. of parameters	736	1051	363	182
No. of restraints	1	1	3	0
H-atom treatment	H atoms treated by a mixture of independent and constrained refinement	H atoms treated by a mixture of independent and constrained refinement	H-atom parameters constrained	H-atom parameters constrained
$\Delta\rho_{max}$, $\Delta\rho_{min}$ (e Å^{-3})	0.32, −0.23	0.19, −0.23	0.28, −0.24	0.11, −0.15
Flack x	−0.2 (10)	−0.1 (11)	0.2 (9)	0.0 (10)

	(9*A*)	(9*B*)	(10*A*)	(10*B*)
Crystal data				
Chemical formula	$C_{14}H_{16}N_2O_2$	$C_{14}H_{16}N_2O_2$	$C_{15}H_{18}N_2O_2$	$C_{15}H_{18}N_2O_2$
M_r	244.29	244.29	258.31	258.31
Crystal system, space group	Monoclinic, $P2_1$	Monoclinic, $P2_1$	Tetragonal, $P4_32_12$	Orthorhombic, $P2_12_12_1$
Temperature (K)	150	150	150	150
a, b, c (Å)	5.6190 (2), 10.0392 (3), 10.7068 (2)	7.8134 (3), 6.5487 (2), 12.1725 (4)	7.8284 (2), 7.8284 (2), 42.8639 (9)	10.1348 (4), 10.9014 (3), 12.1599 (4)
α, β, γ (°)	90, 92.4862 (15), 90	90, 95.0641 (17), 90	90, 90, 90	90, 90, 90
V (Å^3)	603.40 (3)	620.41 (4)	2626.85 (11)	1343.47 (8)
Z	2	2	8	4
Z'	1	1	1	1
μ (mm^{-1})	0.09	0.09	0.09	0.09
Crystal size (mm)	0.25 × 0.30 × 0.40	0.12 × 0.20 × 0.40	0.10 × 0.30 × 0.40	0.25 × 0.30 × 0.35
Data collection				
Diffractometer	Nonius KappaCCD area detector	Nonius KappaCCD area detector	Nonius KappaCCD area detector	Nonius KappaCCD area detector
θ_{max} (°)	27.5	27.5	27.5	27.5
Dataset	−7: 7; −12: 12; −13: 13	−10: 10; −8: 8; −15: 15	−10: 10; −7: 7; −55: 55	−13.0: 13; 0: −14: 14; −15: 15
No. of measured, independent and observed [$I > 2.0\sigma(I)$] reflections	9184, 2749, 2686	9305, 2831, 2604	24 574, 2994, 2402	11 846, 3071, 2577
R_{int}	0.023	0.022	0.055	0.029
Refinement				
$R[F^2 > 2\sigma(F^2)]$, $wR(F^2)$, S	0.027, 0.070, 1.07	0.032, 0.081, 1.05	0.039, 0.091, 1.05	0.036, 0.085, 1.05
No. of reflections	2749	2831	2994	3071
No. of parameters	167	167	173	173

Table 1 (continued)

	(9*A*)	(9*B*)	(10*A*)	(10*B*)
No. of restraints	1	1	0	0
H-atom treatment	H atoms treated by a mixture of independent and constrained refinement	H atoms treated by a mixture of independent and constrained refinement	H-atom parameters constrained	H-atom parameters constrained
$\Delta\rho_{max}$, $\Delta\rho_{min}$ (e Å^{-3})	0.17, −0.14	0.29, −0.19	0.14, −0.14	0.13, −0.19
Flack *x*	−0.2 (8)	−0.1 (9)	1.5 (14)	0.0 (10)

Computer programs: *COLLECT* (Hooft, 1998), *DENZO* (Otwinowski & Minor, 1997), *CAD*4 (Enraf–Nonius, 1994), *JANA*2006 (Petricek *et al.*, 2006), *SIR*92 (Altomare *et al.*, 1994), *SIR*97 (Cascarano *et al.*, 1996), *SHELXL*97 (Sheldrick, 2008).

2. Materials and methods

2.1. Synthesis and structure characterization

The cyclodipeptides (1*A*), (1*B*), (2*A*) and (2*B*), derived from pipecolic acid (Pip), were synthesized in 40–60% yields by coupling optically pure (L or D) *N*-protected amino acids *Z*-Phe-OH or *Z*-(NMe)Phe-OH to the L- or D-pipecolic acid methyl esters with EEDQ (2-ethoxy-1-ethoxycarbonyl-1,2-dihydroquinoline) in dry THF as coupling reagent. The protecting *Z* (benzyloxycarbonyl) group was then removed by HBr/AcOH and cyclization was performed with saturated $NaHCO_3$, according to the procedure described by Anteunis *et al.* (1979). (1*A*): m.p. 423–424 K (from AcOEt–Et_2O); (1*B*): m.p. 407–408 K (from AcOEt – Et_2O); (2*A*): m.p. 408–409 K (from $CHCl_3$–hexane); (2*B*): mp 439–440 K (from $CHCl_3$–hexane).

The synthesis and characterization of (9*A*) and (9*B*) is described by Vicar *et al.* (1973); (9*A*): m.p. 400–401 K (from AcOEt–Et_2O); (9*B*) m.p. 407–409 K (from AcOEt–Et_2O). The synthesis and characterization of (10*A*) is described by Budesinsky *et al.* (1992); m.p. 409 K (from AcOEt–isooctane). Compound (10*B*) was obtained by epimerization of (10*A*) in a $10^{-4}M$ solution of NaOH in CH_3OH at room temperature; m.p. 442 K (from AcOEt–octane).

The structure and purity of all compounds was confirmed by ^{1}H and ^{13}C NMR spectra.

2.2. X-ray structure analysis

Up to now, the crystal structures of several compounds we report here had not been determined. Here we describe the results of novel X-ray structure analyses on (1*A*), (1*B*), (2*A*) and (10*B*).

In addition, new measurements were performed on (2*B*) and (9*B*) for which previously only the positions of heavy atoms were determined (Ramani *et al.*, 1976; Van Poucke *et al.*, 1982), and also on compounds (9*A*) and (10*A*), which have already been published in the literature (Budesinsky *et al.*, 1992; Mazza *et al.*, 1984).

The colorless crystals of (1*A*), (1A^{room}), (1*B*), (2*A*), (2*B*), (9*A*), (9*B*), (10*A*) and (10*B*) were mounted on glass fibers with epoxy cement and measured on a KappaCCD four-circle diffractometer with CCD area detector [(9B^{room}) and (10B^{room}) on a CAD4-MACHIII diffractometer] with Mo $K\alpha$ radiation. The structures were solved with direct methods (*SIR*92; Altomare *et al.*, 1994) and refined by full-matrix least-squares based on F^2 (*SHELXL*97; Sheldrick, 2008); the absorption was neglected. The H atoms on C atoms were recalculated into idealized positions (riding model) and assigned temperature factors $H_{iso}(H) = 1.2U_{eq}$(pivot atom). The H atoms on nitrogen or oxygen were found on difference Fourier maps and refined isotropically. The absolute configuration of all crystals has been assigned by reference to an unchanging chiral center in the synthetic procedure. From the last cycle of refinement of all structures it follows that $(\Delta/\delta)_{max} < 0.001$. Crystallographic data for individual structures are summarized in Table 1. Room-temperature experimental details of (1A^{room}), (9B^{room}) and (10B^{room}) are given in the supplementary material.[1]

The crystals studied, built by molecules of high flexibility, require low-temperature data collection to increase the precision of the structure parameters. However, the low-temperature structures of two crystals [(1*A*) and (1*B*)] exhibit not only the decrease of displacement parameters relative to high-temperature structures [(1A^{room}), (1B^{250})], but also differences in other structural parameters.

The symmetry of structure (1A^{room}) appears to be orthorhombic with the lattice parameters: a = 8.5217 (1), b = 25.0552 (3), c = 13.4521 (2) Å. The orthorhombic lattice is preserved until 250 K. At 240 K the β angle changes from 90 to 90.27 (3)° and the space group from $P2_12_12_1$, Z = 4, to monoclinic $P2_1$, Z = 4. This change is accompanied by a splitting of diffraction peaks. The β angle gradually increases with decreasing temperature, the largest change appearing between 180 and 170 K from 91.17 (3) to 91.27 (3)°. Finally, at 150 K β equals 91.6730 (11)°. This entire process was found to be reversible. The room-temperature and 150 K structures differ mainly in displacement parameters as the uncommonly large displacement parameters of atoms in (1A^{room}) probably result from disorder, which at low temperature splits into two distinct positions of symmetrically independent molecules. Therefore, the reason for $Z' > 1$ in the low-temperature structure is probably kinetic (Hao *et al.*, 2005). Owing to the lack of a sharp boundary between (1*A*) and (1A^{room}), it is not clear whether these changes really constitute a phase transition. Other experiments would be required to resolve this issue, but are outside the scope of this study.

[1] Supplementary data for this paper are available from the IUCr electronic archives (Reference: SO5040). Services for accessing these data are described at the back of the journal.

Also crystal (1*B*) undergoes structural changes, this time accompanied by a change in length of lattice parameters. At 250 K the structure is monoclinic with a = 22.523 (1), b = 6.4103 (3), c = 20.426 (1) Å, β = 105.937 (3)°, Z = 8. The atoms of all four symmetrically independent molecules exhibit very large displacement parameters and the overall low precision of the structure solution ($R[F^2 > 2\sigma(F^2)] = 0.11$) does not allow its publication. Decreasing the temperature, an additional set of diffraction peaks emerges, giving rise to new lattice parameters at 150 K: a = 22.1154 (7), b = 6.3963 (2), c = 29.5771 (7) Å, β = 95.2660 (18)° and six molecules, symmetrically independent in the $P2_1$ space group. Similar to the (1*A*) case, large displacement parameters are still associated with one molecule (see later) at low temperature, indicating persisting disorder. The other five molecules of the unit cell could be well resolved, giving acceptable geometric parameters. An attempt was made to provide a unified description of the phase transition between the low-temperature and room-temperature structures, using the modulation of a small average unit cell. However, this yielded an unreasonable range of C—C bond distances and was therefore abandoned.

2.3. Computational details

Geometry optimizations of the molecules in the gas phase were performed with the *GAUSSIAN*03 package (Frisch *et al.*, 2004). The DFT method with B3LYP functional (Becke, 1996) was used and all atoms were described with the 6-311G(d,p) basis set (Krishnan *et al.*, 1980). The results of these *single molecule* type calculations will be referred to with the 'SM' shorthand. For some systems, the effect of hydrogen bonding on the geometries and energies was examined using a *cluster in vacuo* technique, in which a (central) cyclodipeptide was surrounded with DKP rings of those molecules with which hydrogen bonds are established in the crystal structure. The geometry of the resulting molecular cluster was optimized, but only the atomic coordinates of the central molecule were allowed to relax. The application of constraints on all molecules surrounding the central moiety is necessary to avoid structural collapse of the cluster and ensures that (part of) the crystalline environment is appropriately mimicked for the central cyclodipeptide. However, it must be noted that in this way some of the crystal packing interactions are implicitly taken into account. The shorthand 'HB' was used for this approach. Subsequent energy calculations in the SM and HB scheme were performed using MP2 and the cc-pVDZ basis set (Dunning, 1989), in this way providing a better description of CH$-\pi$ interactions (Tsuzuki *et al.*, 2006).

Finally, the *CPMD* software package (CPMD, 1990–2006) was used to perform DFT simulations of the crystalline state. The BP86 gradient-corrected density functional (Perdew, 1986; Becke, 1992) was used, together with a plane-wave basis set (cut-off 25 Ry) and ultra-soft pseudopotentials of the Vanderbilt type to describe the electron-ion interaction (Vanderbilt, 1990). Periodic boundary conditions were applied on a supercell, which was obtained by duplicating the original crystal unit cell along one axis ($\langle a\rangle$ or $\langle b\rangle$): an $\langle a2bc\rangle$ supercell was used for (1*B*) and (9*B*), whereas a $\langle 2abc\rangle$ supercell was adopted for (1*A*), (2*A*), (2*B*) and (10*B*). This procedure ensured a sufficient sampling of the Brillouin zone in all calculations and is explained in detail in the supplementary material. Periodic geometry optimizations were performed with constant cell dimensions, but no constraints were imposed on the individual atoms. This methodology has been shown to give accurate results in the treatment of organic moieties and molecular crystals at an affordable computational cost (Pauwels *et al.*, 2004).

2.4. Conformational description of cyclodipeptides

2.4.1. Conformation of the DKP ring. The DKP ring can adopt four basic conformation types: planar, chair, boat or twist. The precise conformation of the ring can be determined from the torsion angles φ, ψ, ω which describe the peptide backbone. Their definition is given in Fig. 2. Additional

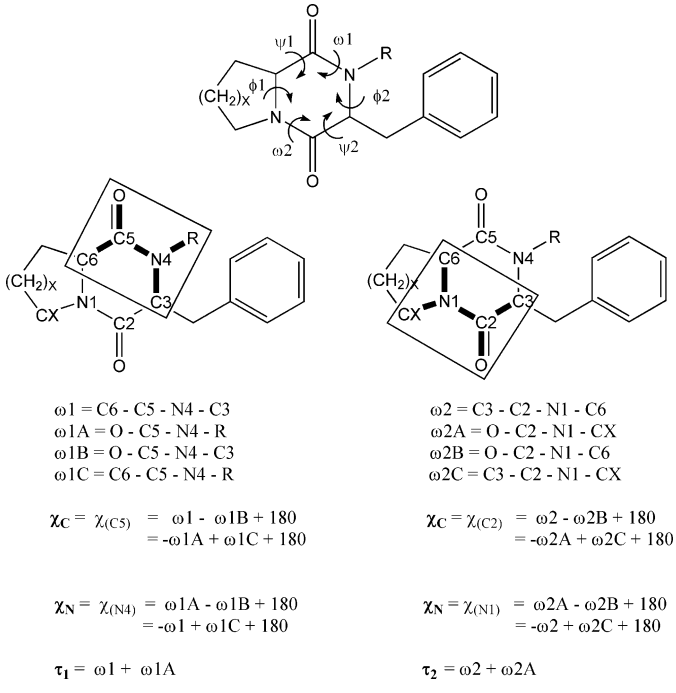

Figure 2
Atom-numbering scheme and definition of torsion angles in the diketopiperazine ring.

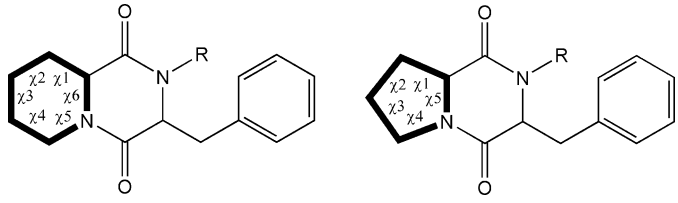

Figure 3
Endocyclic torsion angles in fused six- and five-membered rings of Pip and Pro.

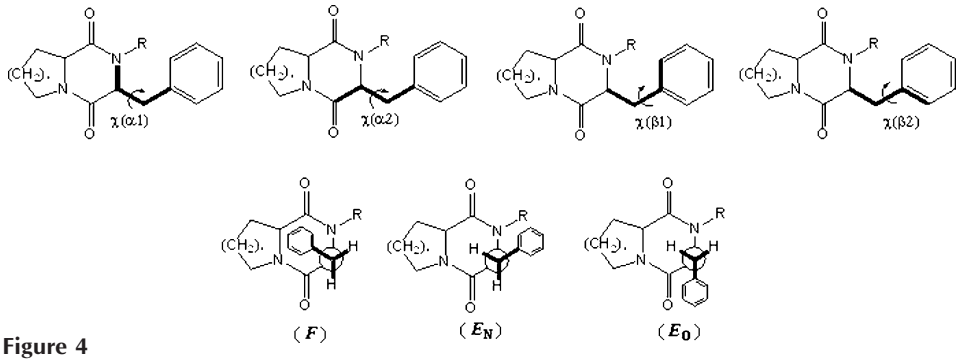

Figure 4
Conformation of the benzyl group of Phe [or (NMe)Phe] – definition of torsion angles and orientation of aromatic ring in staggered rotamers (F, E_N and E_O) as illustrated for L-Phe isomers.

parameters are required for a detailed analysis of the amide bond geometry and its possible deviation from planarity. The parameters χ_C, χ_N and τ – introduced by Dunitz (Winkler & Dunitz, 1971) – define the pyramidalization at the C and N atoms of the amide bond. They can be calculated from a number of dihedral angles (employing the atom-numbering scheme as defined in Fig. 2).

For the comparison of DKP ring geometries we used Ciarkowski's formalism (Jankowska & Ciarkowski, 1987; Gdaniec *et al.*, 1987) describing any feasible conformation as a superposition of the three canonical forms – chair (C), twist (T) and boat (B):

$$T_i = x\cos[2\pi(i-1)/3] - y\sin[2\pi(i-1)/3] + z(-1)^{i-1}, \quad (1)$$

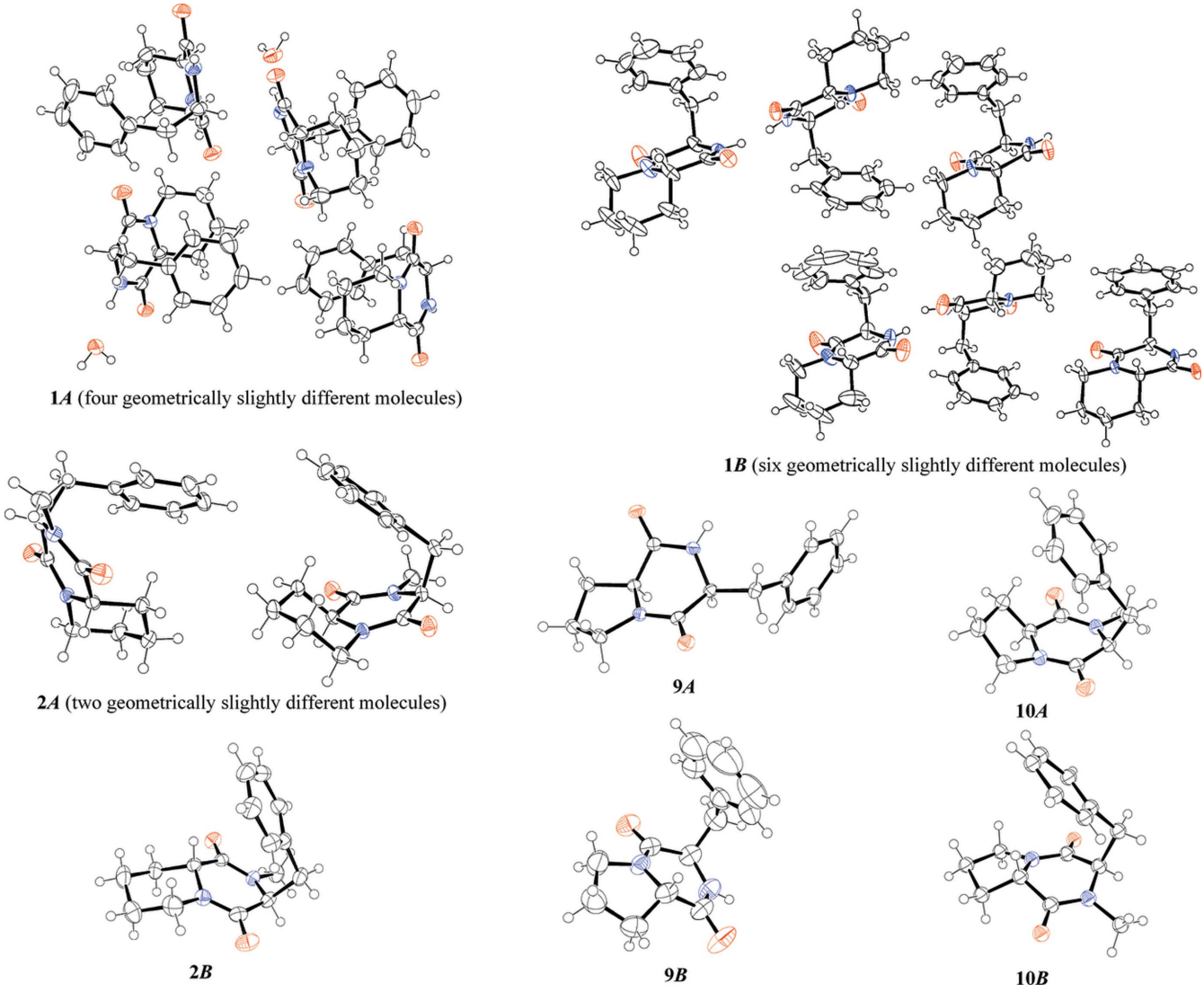

Figure 5
The *ORTEP* views of molecules of cyclodipeptides (1A)–(2B) and (9A)–(10B). Displacement ellipsoids are drawn on the 30% probability level.

Table 2
Torsion angles and Dunitz parameters (Winkler & Dunitz, 1971) obtained from X-ray data of (1*A*)–(2*B*) and (9*A*)–(10*B*) at 150 K.

All angles are in °. Multiple conformers are distinguished by labels m1, ... m6.

	DKP ring						Peptide bond nonplanarity						Pip and/or Pro ring						Phe			
	φ1	ψ1	ω1	φ2	ψ2	ω2	χ(C5)	χ(N4)	τ(1)	χ(C2)	χ(N1)	τ(2)	χ1	χ2	χ3	χ4	χ5	χ6	χ(α1)	χ(α2)	χ(β1)	χ(β2)
(1*A*) c(L-Pip-L-Phe)																						
m1	3.6	−7.4	0.5	9.6	−12.9	6.7	1.1	2.2	2.1	1.6	−1.4	10.4	−54.7	53.4	−53.4	55.1	−59.0	58.6	66.4	−60.2	89.0	−90.3
m2	10.6	−7.7	−4.9	14.7	−11.5	−0.6	−1.0	18.4	9.6	2.6	8.9	5.1	−51.5	51.6	−54.6	58.3	−61.6	57.6	62.5	−64.7	91.8	−85.8
m3	8.0	−8.2	−2.1	12.5	−12.2	2.4	0.8	11.2	6.3	2.6	7.0	9.1	−52.0	52.8	−54.8	57.2	−60.2	56.6	63.8	−64.1	92.3	−85.5
m4	0.0	−3.3	−2.0	9.7	−12.3	8.1	−0.2	20.4	16.6	1.8	−1.0	13.3	−52.9	54.2	−55.6	56.0	−57.0	55.1	66.9	−59.5	90.5	−87.2
(1*B*) c(L-Pip-D-Phe)																						
m1	0.1	−5.2	17.6	−22.6	15.6	−5.9	4.0	−17.1	14.1	−4.4	−0.7	−8.1	−51.8	52.1	−54.3	58.2	−61.1	56.9	−60.2	66.9	92.7	−83.9
m2	13.1	−12.9	16.2	−16.3	13.8	−14.1	4.8	−13.2	14.4	−5.1	8.8	−14.3	−55.3	51.7	−51.1	54.6	−60.5	60.2	−66.2	58.4	88.5	−87.1
m3	3.3	−7.1	15.6	−18.4	13.0	−6.8	3.2	−10.6	17.4	−3.4	3.4	−6.8	−51.0	51.7	−54.2	56.8	−60.1	56.9	−57.0	67.8	91.1	−85.4
m4	6.0	−9.1	17.8	−20.3	15.0	−9.7	2.8	−24.5	8.2	−4.2	2.4	−12.8	−53.9	51.6	−52.8	57.6	−64.0	61.1	−62.4	62.9	89.4	−85.6
m5	7.4	−9.0	16.4	−19.1	15.4	−11.3	3.5	−28.8	0.5	−5.4	2.2	−14.9	−54.2	50.4	−51.5	56.4	−64.5	63.9	−66.2	60.5	87.1	−89.7
m6	7.4	−9.6	16.2	−17.7	13.4	−9.8	4.4	−11.8	16.2	−4.6	4.5	−10.5	−51.4	50.1	−52.1	55.5	−60.0	57.4	−60.2	64.2	87.5	−90.0
(2*A*) c(L-Pip-L-(NMe)Phe)																						
m1	16.4	−3.4	−16.4	23.4	−10.0	−9.2	−3.8	13.3	−15.7	−0.1	11.2	−7.1	−54.0	52.6	−54.0	55.6	−59.2	58.7	66.4	−61.6	89.3	−89.7
m2	18.1	−3.3	−17.6	24.2	−9.2	−11.3	−4.4	13.2	−17.6	−0.8	12.1	−9.7	−54.2	52.9	−53.6	55.1	−59.6	59.0	65.2	−63.4	91.0	−88.6
(2*B*) c(D-Pip-L-(NMe)Phe)																						
	17.7	−10.7	−10.7	25.1	−17.6	−3.2	−2.2	9.4	−9.6	1.6	15.4	7.4	53.7	−56.1	56.4	−55.5	56.2	−54.2	67.6	−59.6	89.3	−86.5
(9*A*) c(L-Pro-L-Phe)																						
	−45.0	46.7	−0.8	−48.5	50.1	−4.2	1.2	8.6	5.7	−1.6	2.7	−4.2	−28.0	37.4	−31.7	14.6	8.5	–	−80.0	156.5	117.7	−61.6
(9*B*) c(L-Pro-D-Phe)																						
	−16.3	15.6	0.3	−16.2	15.4	0.3	−0.7	2.2	3.5	−1.1	5.1	5.2	−39.0	34.6	−16.8	−8.6	30.1	–	−78.3	49.0	81.3	−96.4
(10*A*) c(L-Pro-L-(NMe)Phe)																						
	6.3	4.2	−19.4	23.5	−11.9	−1.8	−4.9	14.2	−19.8	2.9	23.2	16.6	−36.0	23.1	−1.4	−22.6	37.4	–	64.7	−62.6	90.2	−89.8
(10*B*) c(L-Pro-D-(NMe)Phe)																						
	−28.0	25.6	1.8	−28.2	26.0	1.4	−0.8	−4.7	−0.3	0.0	3.7	6.7	−38.4	39.6	−24.9	0.3	24.3	–	−67.7	60.4	87.6	−90.3

where T_i are either endocyclic torsion angles α_i or the displacements of the ring atoms i (1, 2, 3, ... 6). x, y and z represent the contributions of the respective canonical forms: z is a measure of the chair character, whereas x and y describe the twist-boat character in the pseudorotational plane. From the observation of a clustering of x and y coordinates in a set of 65 experimental DKP X-ray structures reviewed by Ciarkowski (Jankowska & Ciarkowski, 1987; Gdaniec *et al.*, 1987), it was proposed to change (specifically for the diketopiperazine) the x, y, z ring-puckering coordinate system to the l, t, z coordinate system, by performing a 23.3° counterclockwise rotation about the z axis. For reasons of comparability with this prominent review, we also apply this coordinate transformation when reporting our data.

In semispherical coordinates ζ, λ and η (latitude, longitude and amplitude) the endocyclic torsion angles α_i of the DKP ring are to a very good approximation generated by

$$\alpha_i = \eta_{T/B}\cos[\lambda + 2\pi(i-1)/3] + (-1)^{i-1}\eta_C \quad \text{with } i = 1, 2, 3, \ldots 6\ (\varphi_1, \psi_1, \omega_1, \varphi_2, \psi_2, \omega_2), \qquad (2)$$

where $\eta_{T/B} = \eta\cos\zeta$ and $\eta_C = \eta\sin\zeta$ are the contributions of the twist-boat and chair forms to the puckering amplitude η, and λ is the phase angle of pseudorotation. The relative contribution of the chair form X_C is expressed as $X_C = |\eta_C|/(|\eta_{T/B}| + |\eta_C|)$.

2.4.2. Conformation of the fused six- or five-membered ring. Endocyclic torsion angles χ1 to χ6 (for Pip) and χ1 to χ5 (for Pro) are used to describe the conformation of these rings. Their definition is given in Fig. 3.

2.4.3. Conformation of the benzyl group of Phe (or NMe-Phe). The side-chain conformation is described by torsion angles $\chi(\alpha1)$ = N—C_α—C_β—C_{ipso}, $\chi(\alpha2)$ = C′—C_α—C_β—C_{ipso}, $\chi(\beta1)$ = C_α—C_β—C_{ipso}—C_{ortho} and $\chi(\beta2)$ = C_α—C_β—C_{ipso}—C_{ortho} (Fig. 4). The three energetically favored staggered rotamers for the orientation of Phe ring are denoted as F (folded), E_N (extended to amide nitrogen) and E_O (extended to amide oxygen), which is independent of the Phe configuration.

3. Results and discussion

3.1. Overview and comparison of crystal structures

A quite remarkable feature in three of the determined crystal structures is that a number of different molecular conformations (Z') are present within the asymmetric unit cell: four in (1*A*), six in (1*B*) and two in (2*A*). In Figs. 5(*a*) and

(*b*) the symmetry-independent molecules of these compounds are illustrated, along with those of cyclodipeptides (2*B*) and (9*A*)–(10*B*). All the main torsion angles and Dunitz parameters describing the conformation of the individual molecules in the studied crystals are given in Table 2. There are no significant distortions of bond lengths or bond angles in the entire series. The conformational properties of the crystalline cyclodipeptides (1*A*)–(2*B*) and (9*A*)–(10*B*) are only briefly discussed in the following paragraph. A detailed overview is presented in the supplementary material.

3.1.1. Side-chains. The six-membered piperidine ring of pipecolic acid retains a chair-form $_{\gamma}C^{N}$ in (1*A*)–(2*B*). Its conformation is not influenced by the relative configuration of the residues or by *N*-methylation. The five-membered pyrrolidine ring of Pro, on the other hand, is known to be relatively flexible. All possible proline conformations can be described by a phase angle *P* and a maximum pucker amplitude τ_{m} in a pseudorotation pathway, as described by de Leeuw *et al.* (1983). The phase angle in (9*A*)–(10*B*) lies in a relatively small interval of 60°. They all belong to *N*-type conformers with phase angles *P* of 5° ($^{\gamma}T_{\beta}$), −30° ($^{\alpha}T_{\beta}$), −53° ($^{\alpha}E$) and −17° ($_{\beta}E$) for (9*A*), (9*B*), (10*A*) and (10*B*), and maximum pucker amplitudes between 37 and 40°.

In nearly all of the cyclodipeptides (1*A*)–(2*B*) and (9*A*)–(10*B*), the aromatic ring of Phe (or NMe-Phe) is folded over the DKP ring with $\chi(\alpha)$ absolute values between 57 and 75° (*F* conformer, as depicted in Fig. 4). Only in (9*A*) the aromatic ring adopts the E_{N} orientation with $\chi(\alpha) \simeq -80°$. Possible explanations will be discussed below.

3.1.2. DKP ring conformation. From previous NMR and X-ray studies the primary factors that shape the DKP ring in cyclodipeptides are well recognized and have been reviewed (Anteunis, 1978; Jankowska & Ciarkowski, 1987; Gdaniec *et al.*, 1987). In this paragraph we give a brief survey. In bicyclic cyclodipeptides (1*A*)–(2*B*) and (9*A*)–(10*B*), the DKP and piperidine (or pyrrolidine) rings are fused, sharing the N and Cα atoms. As such, the endocyclic torsion angles at the ring junction – ϕ1 and χ6 (or χ5) – are interdependent. The ring size of the cyclic imino acid therefore limits the range of accessible ϕ1 for the DKP ring. Fusion to a six-membered ring imposes low ϕ1 values, *i.e.* a flattening of the DKP ring, while fusion to a five-membered ring typically puckers the DKP ring by 30–40° with the Cα—Cβ bond in a pseudo-equatorial position. However, the approximate relation $|\chi - \phi| \simeq 60°$ for a planar amide N is considerably relaxed for a pyramidal amide N typical of non-planar amide bonds. As amino acid side-chains in general, the benzyl group of Phe prefers the pseudo-axial orientation creating local pucker with opposite signs of ψ2 and ϕ2 to escape repulsion with the vicinal carbonyl group. This tendency to tilt the benzyl side-chain to the axial position is further enhanced by *N*-methylation, thus avoiding repulsion between the vicinal methyl and benzyl groups. There is convincing evidence from NMR and X-ray data and from theory that aromatic side-chains *in pseudo axial orientation* prefer the folded rotamer *F* as the result of a face-to-face attractive interaction with the DKP ring, with an optimal ϕ2 (absolute) value of *ca* 20°.

The conformation of the DKP ring of all compounds (1*A*)–(2*B*) and (9*A*)–(10*B*) is represented graphically in Fig. 6 in terms of the conformational parameters *l*, *t* and *z* (Jankowska & Ciarkowski, 1987; Gdaniec *et al.*, 1987).

Many of the eye-catching conformational features of the present series of cyclodipeptides can be interpreted by a combination of the above-mentioned specific constraints imposed by the cyclic and the benzylic side-chains. Since the puckering characteristic for each side-chain can displace the Cα atoms either to the same side or to the opposite side of the average ring plane depending on the relative configuration of the two residues, the resulting conformational preference of the DKP ring can be substantially different in *cis* (LL) and *trans* (LD) series.

In the pipecolic acid (Pip) analogs (1*A*)–(2*B*) the DKP ring is rather flat at the ring-junction, as expected, and slightly or moderately puckered at the Phe side to allow for the favorable stacking of the phenyl group over the DKP ring. The *N*-methylation increases the puckering amplitude [comparing (1*A*) with (2*A*), and (1*B*) with (2*B*)], with a concomitant shift of phase angle (see Fig. 6 and detailed overview of conformational properties in the supplementary material) only in the *cis* analogs.

In the *trans* proline analogs (9*B*) and (10*B*) both side-chains are compatible with a moderately puckered $_{C\alpha}B$ boat conformation with nearly planar amide bonds and the phenyl group again stacking over the DKP ring. *N*-Methylation increases the buckle of this boat conformation slightly. This strongly contrasts with the dramatic effect of *N*-methylation in the *cis* proline analogs. In (9*A*) the $_{C\alpha}B$ form is preserved

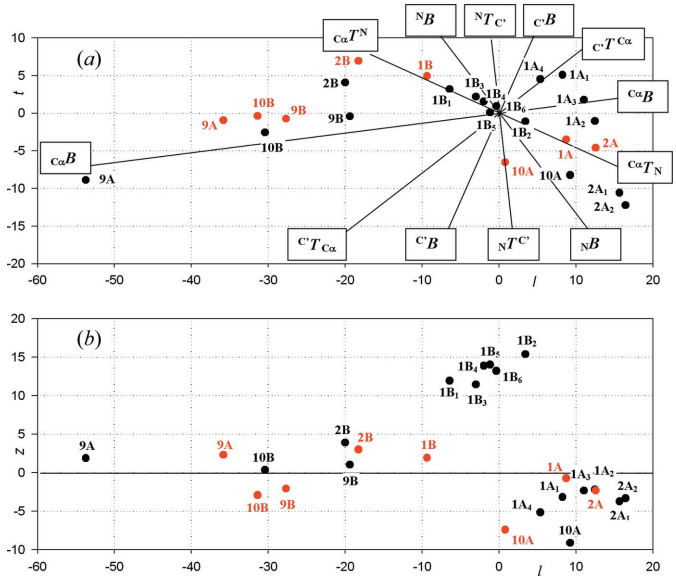

Figure 6
Graphical representation of experimental X-ray (in black) and calculated single molecule (in red) conformations of the DKP ring in (1*A*)–(2*B*) and (9A)–(10*B*). (*a*) The *l*,*t* plot showing the twist-boat character in the pseudorotational plane. (*b*) The *l*,*z* plot showing the contribution of chair character expressed as the parameter *z*, perpendicular to the *l*,*t* plane, and directly related to η_{C}. For (2*B*) the signs of *l*, *t* and *z* parameters were changed due to the D-configuration of the Pip residue.

despite the mutually eclipsed position of the benzyl and carbonyl groups in the pseudo-equatorial position. In (10*A*) the additional repulsion with the *N*-methyl group inverts the pucker in the $\psi 2$, $\phi 2$ region to the benzyl's preference, as such compromising with amide bond non-planarity and appreciable chair character.

Several facts however remain not well understood: the pronounced pucker of the (9*A*) $_{C\alpha}B$ boat and its preference for the E_N rotamer, the occurrence of multiple conformers in the crystals of (1*A*), (1*B*) and (2*A*), and the details of amide bond deviations from planarity. A more advanced analysis requires the separation of intra- and intermolecular effects. In the following, this will be done by comparing the X-ray structures with *ab initio* calculations. First we will discuss the individual crystal structures.

3.2. Hydrogen bonding and molecular packing

3.2.1. *cyclo*(L-Pip-L-Phe) (1*A*). The crystal structure of (1*A*) shows four geometrically slightly different molecules of c(L-Pip-L-Phe) in the asymmetric unit and two water molecules (Fig. 5). The hydrogen-bonding network in the crystal (see Fig. 7) interconnects four slightly different DKP conformers (m1, m2, m3, m4) and two different water molecules (w1, w2). Three hydrogen bonds involving the secondary amide bonds of m1 and m2 and a w2 water molecule form a ten-membered ring. A similar feature is present between molecules m3, m4 and w1. These rings are connected to each other by hydrogen bonds between water molecules and the Phe carbonyls of m1 and m4.

This hydrogen-bonding network extends as a helix along the *a* axis of the unit cell, thus forming a chain (seen in cross-section in Fig. 8), centering the water molecules, all $\omega 1$ bonds and the Phe carbonyls of m1 and m4 into one big polar interior region. This chain is further stabilized by four non-classical hydrogen bonds between the Pip carbonyl oxygen and C—H_α or C—H_β of Phe. The exterior of this helical chain exposes all non-polar Phe and Pip side-chains and the Phe carbonyls of m2 and m3. Anti-parallel packing of chains in the crystallographic *b* direction is facilitated by non-classical hydrogen bonds between the Pip carbonyl oxygen (of m2 and m3) and the *meta*-C—H of Phe. Parallel packing of chains along the crystallographic *c* axis involves dispersion-type contacts between the Pip and Phe side-chains.

3.2.2. *cyclo*(L-Pip-D-Phe) (1*B*). The unit cell of compound (1*B*) contains 12 molecules related by $P2_1$ symmetry along the *b* direction. Six geometrically slightly different molecules are observed in the asymmetric unit (see Fig. 5 and Table 2). Based on similarity between the hydrogen-bond network the compounds cluster in pairs m1–m2, m3–m4 and m5–m6. A similar hydrogen-bond network is present in each pair (schematically shown in Fig. 7), giving rise to three slightly different parallel chains in the direction of the crystallographic *b* axis. These chains have a polar interior containing the hydrogen-bonded secondary amide bonds, whereas the non-polar Phe and Pip side-chains are pointing outwards. Each chain has two slightly different molecules that alternate (*e.g.* . . . –m1–m2–m1–m2– . . .) and wind around an approximate twofold screw axis, a phenomenon known as *pseudo*-symmetry. The six slightly different conformers pack very efficiently in the *b* direction at the common distance of 6.40 Å, the *b* unit-cell length. Fig. 9 illustrates the packing of the three different chains in the *ac* plane. Another distinct characteristic in the crystal structure of (1*B*) is the packing of the phenyl groups of different chains which enter in *herringbone* motifs, extending the chains in the crystallographic *a* direction to form layers. Three such different layers pack in the *c* direction making non-polar contacts between the Pip and Phe side-chains (see Fig. 9*b*). One layer is formed with m1–m2 chains only, with phenyl herringbone motifs between identical molecules (m1 with m1, m2 with m2). The second layer alternates m3–m4 chains and m5–m6 chains by herringbone motifs between different molecules (m4 with m5, m3 with m6). The third layer is like the second one but rotated by 180°. The slight geometrical differences are obviously induced by different intermolecular contacts between chains.

3.2.3. *cyclo*(L-Pip-L-(NMe)Phe) (2*A*). The unit cell of (2*A*) contains two geometrically slightly different molecules (Fig. 5). Here again $Z' > 1$ is observed in a low-symmetry space group *P*1. Tertiary amide bonds exclude the presence of

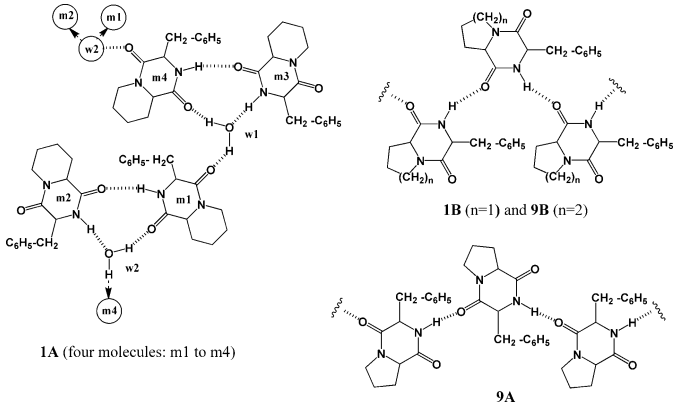

Figure 7
The types of hydrogen bonding observed in the crystal structures of (1*A*), (1*B*), (9*A*) and (9*B*).

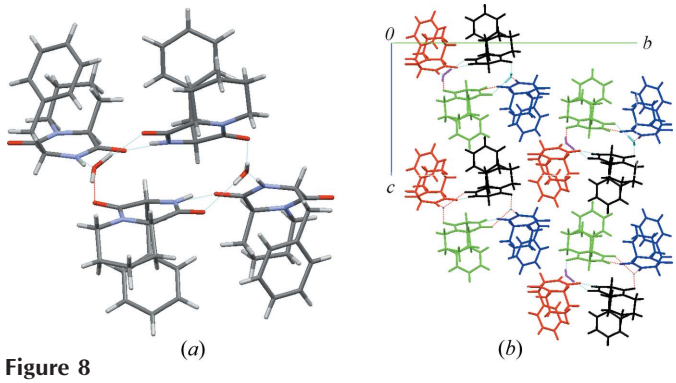

Figure 8
Molecular packing of *cyclo*(L-Pip-L-Phe) (1*A*) in the crystal seen along the crystallographic *a* axis: (*a*) hydrogen-bond chain colored by elements; (*b*) parallel and anti-parallel packing of chains in the *c* and *b* directions of the unit cell, with molecules colored by symmetry equivalence (m1 green, m2 blue, m3 red, m4 black).

classical hydrogen bonds. However, each of these two molecules is involved in a two-dimensional network with six short contacts (penetrations from 0.24 to 0.30 Å) of the C—H···O type with five neighboring molecules. These short contacts generate double layers within the crystal parallel with the *ab* plane, linking a layer of m1 to a layer of m2 molecules. Each double layer has a polar interior and the non-polar side-chains of the cyclodipeptides point outwards along the *c* direction. These double layers stack along the *c* direction without short contacts, but close packing is achieved by a maximal fitting of hollows into the bumps, as illustrated in Fig. 10.

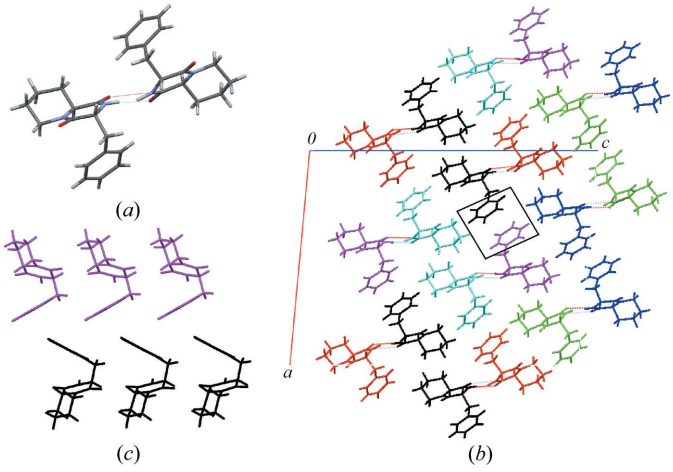

Figure 9
Molecular packing of *cyclo*(L-Pip-D-Phe) (1*B*): (*a*) One of the three similar chains (m5–m6) formed by hydrogen bonding extending and viewed along the *b* axis; (*b*) packing of three chains in the *a* direction. Phenyl/phenyl herringbone motifs extend the chains in the *a* direction to form layers. Three layers pack to complete the unit cell along its *c* axis (m1 green, m2 blue, m3 red, m4 black, m5 pink, m6 turquoise). (*c*) Herringbone stacking of the phenyl groups highlighted with a box in (*b*).

3.2.4. *cyclo*(D-Pip-L-(NMe)Phe) (2*B*). The unit cell of (2*B*) contains four molecules with identical conformations (Fig. 5). The space group is $P2_12_12_1$. Classical hydrogen bonds are again excluded, but each molecule has eight short contacts (penetrations from 0.14 to 0.42 Å) of the C—H···O type with six other molecules. Molecular packing results in a three-dimensional-network as shown in Fig. 11.

3.2.5. *cyclo*(L-Pro-L-Phe) (9*A*). Two molecules of (9*A*) in the unit cell are related *via* a twofold screw axis (space group $P2_1$). Each molecule in addition to two classical hydrogen bonds has 16 short intermolecular contacts with four neighboring molecules resulting in remarkably high packing density (1.32 g cm^{-3}). Comparison of previously reported X-ray data at room temperature (Mazza *et al.*, 1984), at 100 K (Meetsma, 2006) and at 150 K (this paper) shows that no phase transition takes place that could lead to structure modulation.

The crystal packing of (9*A*) is characterized by an infinite chain of hydrogen bonds (2.97 Å, schematically shown in Fig. 7) between NH and the C=O group of the Phe residue along a twofold screw axis in the *b* direction. A non-classical hydrogen bond between H-β of Phe and the carbonyl oxygen of Pro (H···O distance 2.68 Å) enforces this chain motif. Seen along the *c* direction these hydrogen-bond chains have wave-like shapes (see Fig. 12) that pack in parallel orientation to form double layers parallel to the crystallographic *ab* plane of the unit cell. These double layers have polar interiors of DKP rings involved in hydrogen bonds and amide–amide interactions, but have exclusively non-polar side-chains at the outside, allowing their packing in the *c* direction by London dispersion forces. Each molecule fits the cleft formed by three successive residues of the neighboring chain remarkably well, as shown by the close contacts shown in Fig. 12(*c*) and mapped in color code on the Hirshfeld surface in Fig. 12(*d*) (McKinnon *et al.*, 2007). In fact, Hα—Cα—C=O moieties of Pro and Phe of interacting molecules make a series of (six) close contacts in

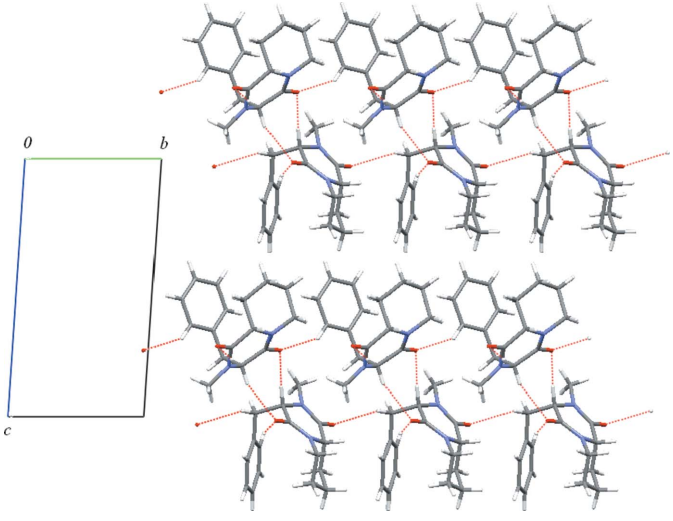

Figure 10
Molecular packing of *cyclo*(L-Pip-L-(NMe)Phe) (2*A*) in the crystal (view along *a* axis). Intermolecular contacts shorter than ΣVdW = 0.1 Å are indicated by dotted red lines.

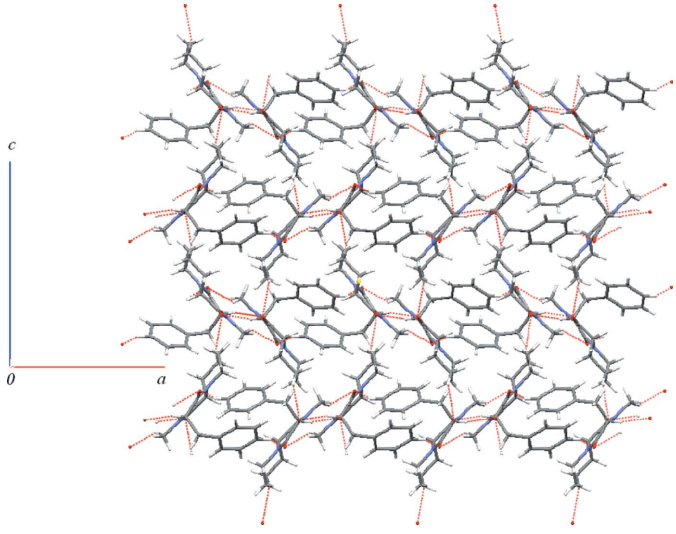

Figure 11
Molecular packing of *cyclo*(D-Pip-L-(NMe)Phe) (2*B*) in the crystal viewed along the *b* axis. Intermolecular contacts shorter than ΣVdW = 0.1 Å are indicated by dotted red lines.

a binding motif composed of two C_α—H···O interactions (H···O distances 2.65 and 2.53 Å) and a C═O/C═O dipole/dipole interaction (C···O distances of 3.10 and 3.05 Å). As the depth and width of the cleft formed by three successive molecules in a chain is determined by the buckle of the DKP ring and the tendency of the hydrogen bonds to be linear, we propose that the peculiar conformation of (9*A*) with extremely high pucker (high φ and ψ values) of the DKP ring is stabilized by the combination of strong NH···O hydrogen bonds and C═O/C═O dipole/dipole attractions.

3.2.6. *cyclo*(L-Pro-D-Phe) (9*B*). There are two geometrically identical molecules of (9*B*) found in the unit cell (Fig. 5). Each molecule has two classical hydrogen bonds with neighboring molecules involving the carbonyl group of Pro and the NH group of Phe, *i.e.* the C═O and NH groups of the same amide bond (see Fig. 7). Not only the hydrogen-bonding scheme, but also the space group ($P2_1$) and the packing mode of (9*B*) are identical with its homologue (1*B*), including the twofold screw axes and herringbone motifs. However, the asymmetric unit of (9*B*) contains only one conformer. Short contacts with the other six molecules led to the three-dimensional network of parallel chains, as shown in Fig. 13.

3.2.7. *cyclo*(L-Pro-L-(NMe)Phe) (10*A*). Each of eight molecules of (10*A*) in the unit cell assumes the same conformation (Fig. 5). The space group is $P4_32_12$. There are no classical hydrogen bonds but several relatively weak to medium contacts are present of the C—H···O and C—H···π type. The overall molecular packing is comparable to (2*A*). The polar contacts (mainly involving the DKP and pyrrolidine rings) and non-polar contacts (between the benzyl sidechains) segregate in similar double layers parallel to the *ab* plane. Four 'double' layers are close-packed (by phenyl/phenyl contacts) in the *c* direction, each double layer rotated by 90° about the *c* axis, shown in Fig. 14.

3.2.8. *cyclo*(L-Pro-D-(NMe)Phe) (10*B*). The unit cell contains four molecules of (10*B*) with an identical conformation (Fig. 5). Each has six medium to strong contacts of the C—H···O type and two interactions of the C—H···π type. The molecular packing in the crystal is shown in Fig. 15. Compounds (2*B*) and (10*B*) not only have similar molecular shapes, but crystallize in the same space group, $P2_12_12_1$, each with four identical molecules in their unit cell. In both crystal structures polar and non-polar short contacts are not segregated, but rather evenly contribute to packing in three dimensions.

An overall picture of crystal packing forces in the crystals of (1*A*)–(2*B*) and (9*A*)–(10*B*) can be obtained with the program *CrystalExplorer*, mapping close intermolecular contacts on the Hirshfeld surface (Spackman & McKinnon, 2002) and sorting them according to atom types (see supplementary material). To a first approximation and excluding (9*A*), dispersion type H···H contacts are covering approximately 67% of the molecular surface. Hydrogen bonds of the classical type NH···O and non-classical type CH···O sum up to H···O contacts that cover *ca* 20% in all systems. Alkyl···aryl interactions represented as H···C contacts amount to 10%, again with (9*A*) as the exception. The crystal of (9*A*) is atypical in this series with an increased contribution of the alkyl/aryl interactions (17%) at the expense of dispersion contacts, and a remarkable 1.5% O···C contact due to dipole/

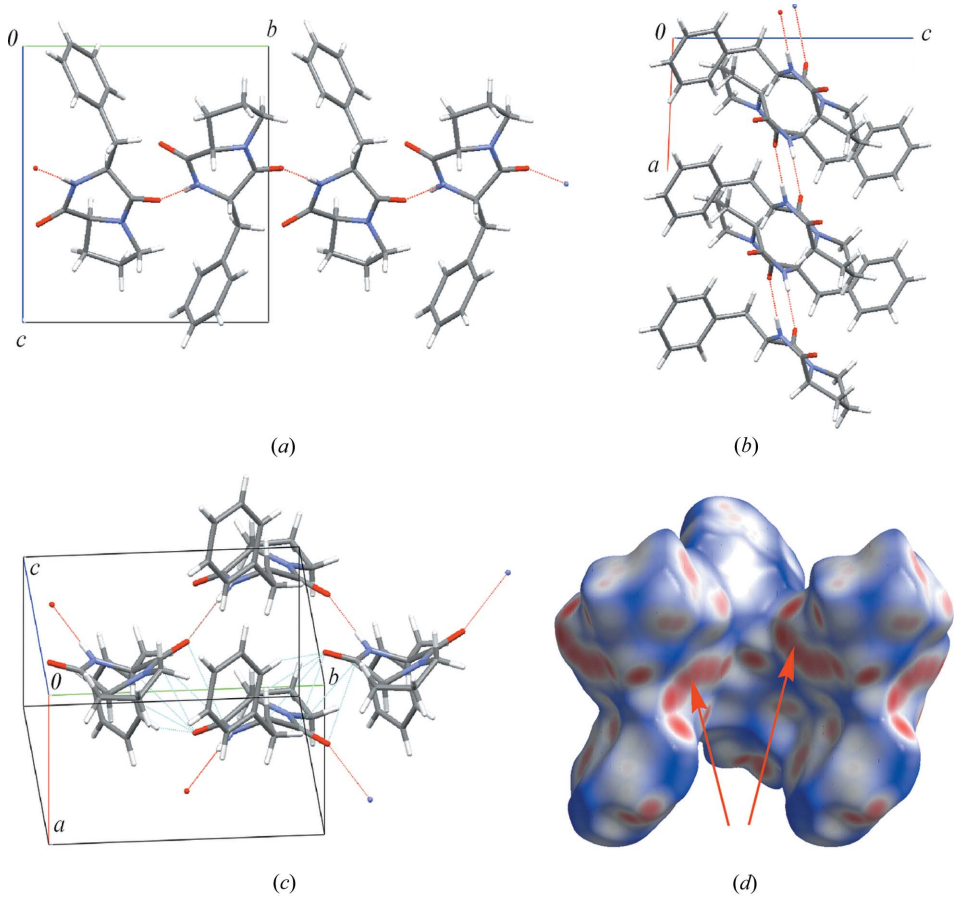

Figure 12
Molecular packing of *cyclo*(L-Pro-L-Phe) (9*A*) in the crystal: (*a*) view along the *a* axis; (*b*) view along the *b* axis; (*c*) the central molecule (lower chain) fits precisely into the cleft formed by the three molecules of the upper chain; hydrogen bonds are in red and binding contacts in the cleft are colored blue; the hydrogen-bond extensions to neighboring units underline the wave-like shape; (*d*) view along the *a* axis into the empty cleft showing the normalized contact distance d_{norm} mapped on the Hirshfeld surface in color code (McKinnon *et al.*, 2007). Two patches of red spots (indicated with red arrows) show the imprints of the Hα—Cα—C═O binding motifs.

dipole interaction between amide carbonyl groups.

The impact of *N*-methylation is evident. Strong and directional NH···O hydrogen bonds dominate the packing in crystals of compounds (1*A*), (1*B*), (9*A*) and (9*B*). Although saturation of the hydrogen-bonding capacity of the secondary amide N—H could be easily achieved by the formation of dimers, in the present series linear chains are preferred irrespective of the size of the fused rings and the relative configuration of the chiral centers.

Two distinct types of hydrogen-bond chains can be formed. Chains that link OCNH···OCNH moieties involving the same amide bond appear in *cyclo*(L-Pip-D-Phe) (1*B*) and *cyclo*(L-Pro-D-Phe) (9*B*) and in the alkyl analogs *cyclo*(L-Pro-D-Leu) (Hendea *et al.*, 2006), *cyclo*(L-Pro-L-Ala) (Cotrait & Leroy, 1979; Hendea *et al.*, 2006). These are typically right-handed helices for L-imino residues (Pro or Pip) and have a short pitch of 6.2–6.8 Å. Chains that link $OCC_{\alpha}NH\cdots OCC_{\alpha}NH$ moieties involving NH and O=C groups of the same amino acid residue appear in *cyclo*(L-Pro-L-Phe) (9*A*) and the alkyl analogs *cyclo*(L-Pro-L-Leu) (Karle, 1972; Hendea *et al.*, 2006), *cyclo*(D-Pip-L-Leu) (Symerský *et al.*, 1987) and *cyclo*(L-Pip-L-Val) (Lenstra *et al.*, 1991). These helices are typically left-handed for L-imino acid residues (Pro or Pip) and have a pitch of 9.5–11 Å. The two categories of chains are represented by *cis* as well as *trans* isomers of both *cyclo*(Pro-Xxx) and *cyclo*(Pip-Xxx) members. Into which type of hydrogen-bond chain a specific cyclic dipeptide crystallizes is therefore not simply related to ring size and stereochemistry, but is rather a complex function of molecular shape and flexibility and of all intermolecular interactions.

The *N*-methylated *cis* analogs (2*A*) (space group *P*1) and (10*A*) ($P4_32_11$) form double layers (with polar DKP rings inside and non-polar side-chains outside), in contrast to the *trans* isomers (2*B*) and (10*B*) (both $P2_12_12_1$) which show a more isotropic distribution of the type and strength of contacts in the three dimensions. In this context it is notable that the single molecule simulations of the *trans* isomers (2*B*) and (10*B*) deviate less from the crystal conformations (DKP ring $\Delta_{av} \simeq 2.0$ and 3.0°) than the *cis* isomers (2*A*) and (10*A*) ($\Delta_{av} \simeq 4.65$ and 5.97°), suggesting that the more 'isotropic' crystal environment has a smaller impact on molecular conformation.

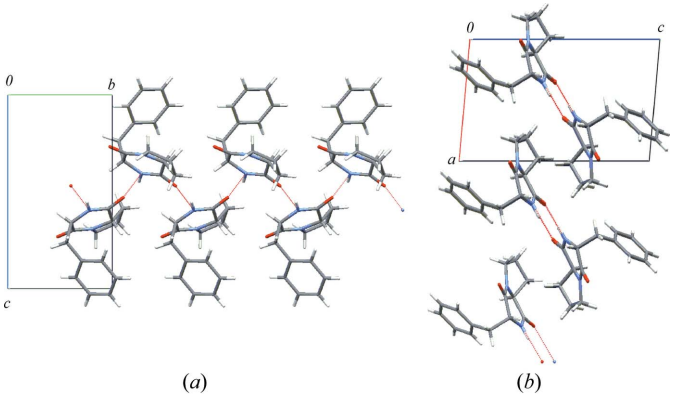

Figure 13
Molecular packing of *cyclo*(L-Pro-D-Phe) (9*B*) in the crystal: (*a*) view along the *a* axis; (*b*) view along the *b* axis. The hydrogen bonds are indicated by red dotted lines.

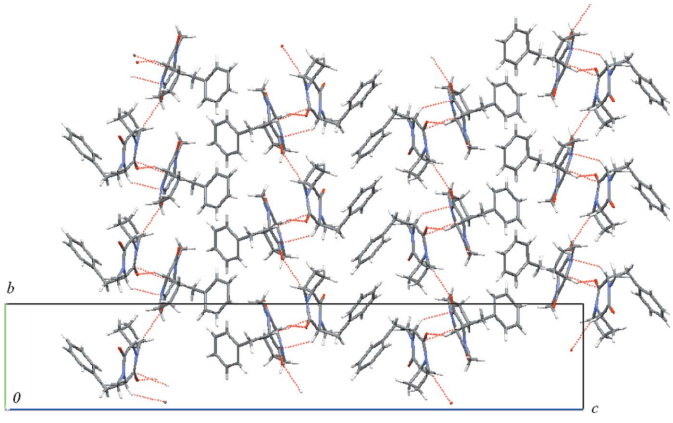

Figure 14
Molecular packing of *cyclo*(L-Pro-L-(NMe)Phe) (10*A*) in the crystal: view along the *a* axis. Intermolecular contacts shorter than ΣVdW = 0.1 Å are indicated by red dotted lines.

3.3. Single molecule calculations

The SM optimizations (see Tables 3 and 4) indicate what the conformational preference of a particular DKP molecule is in the absence of any intermolecular interactions. This conformation is never identical to that observed in the crystal, but the observed difference varies from rather small [(10*A*), (10*B*)] to very big [(1*A*), (1*B*), (9*A*)]. Since SM calculations

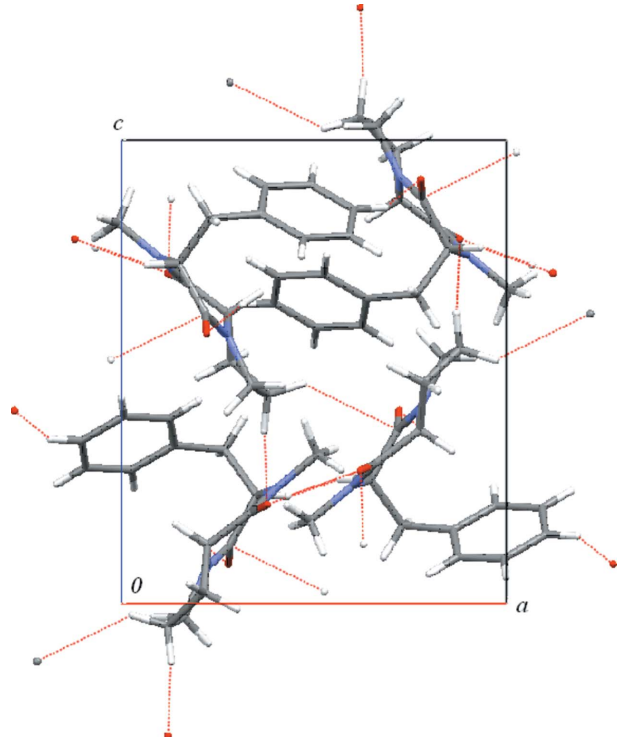

Figure 15
Molecular packing of *cyclo*(L-Pro-D-(NMe)Phe) (10*B*) in the crystal: view along the *b* axis Intermolecular contacts shorter than ΣVdW = 0.1 Å are indicated by red dotted lines.

Table 3
Torsion angles of the DKP ring, Pip ring and Phe side-chain and peptide bond non-planarity parameters (in °) for (1*A*)–(2*B*) as obtained by single molecule (SM) and periodic (⟨2*ab*⟩) DFT calculations.

Δ_{av} is the average deviation between calculated and experimental X-ray angles inside each group and Δ_{max} is the largest group difference (values in parentheses). The notations m1–m6 correspond to the symmetry-independent molecules in the unit cell.

		DKP ring						Peptide bond nonplanarity						Pipecolic acid ring						Phe			
Method	Mol.	ϕ_1	ψ_1	ω_1	ϕ_2	ψ_2	ω_2	χ(C5)	χ(N4)	τ(1)	χ(C2)	χ(N1)	τ(2)	χ1	χ2	χ3	χ4	χ5	χ6	χ (α1)	χ (α2)	χ (β1)	χ (β2)
(1*A*) c(L-Pip-L-Phe)																							
SM		9.0	−4.4	−5.3	10.4	−5.5	−3.8	−1.1	4.3	−5.2	−0.1	4.9	−2.6	−54.5	53.3	−53.0	53.7	−57.3	57.6	65.6	−62.8	91.3	−88.1
Δ_{av}	m1			5.48 (10.5)						5.42 (13.0)						0.82 (1.7)					1.98 (2.6)		
	m2			3.12 (6.0)						7.23 (14.8)						2.53 (4.6)					1.95 (3.1)		
	m3			3.85 (6.8)						6.12 (11.7)						2.07 (3.6)					1.68 (2.6)		
	m4			5.45 (11.9)						10.47 (21.8)						1.72 (2.7)					1.58 (3.3)		
⟨2*ab*⟩	m1	5.5	−9.2	1.1	10.3	−13.6	6.1	0.1	6.7	8.9	2.3	0.1	10.0	−55.4	53.2	−52.7	53.8	−58.4	59.4	66.6	−61.4	88.6	−88.9
	m2	10.2	−8.6	−4.7	16.3	−14.2	1.5	−0.6	11.6	2.7	2.4	7.7	8.3	−51.4	51.6	−54.6	57.2	−59.7	56.7	61.4	−66.2	93.0	−84.7
	m3	7.4	−8.6	−1.6	12.7	−13.3	3.7	0.2	10.6	7.3	3.0	6.0	10.4	−51.7	52.5	−55.3	57.1	−59.1	56.2	62.7	−64.7	92.9	−84.5
	m4	0.5	−4.4	−1.5	10.4	−13.5	8.7	−0.2	8.2	5.4	3.0	−1.7	12.8	−53.2	53.6	−54.9	55.4	−57.5	56.3	67.7	−59.7	90.2	−86.4
Δ_{av}	m1			1.05 (1.9)						2.50 (6.9)						0.73 (1.3)					0.55 (1.2)		
	m2			1.33 (2.7)						3.12 (6.9)						0.67 (1.9)					1.22 (1.5)		
	m3			0.67 (1.3)						0.80 (1.3)						0.45 (1.1)					0.82 (1.1)		
	m4			0.75 (1.2)						4.28 (12.2)						0.67 (1.2)					0.52 (0.8)		
(1*B*) c(L-Pip-D-Phe)																							
SM		−9.4	3.2	8.2	−13.2	6.4	4.3	1.3	−8.4	6.7	−0.4	−9.2	−0.2	−53.8	54.3	−53.9	53.8	−55.9	55.3	−65.0	62.9	89.5	−89.8
Δ_{av}	m1			9.18 (9.5)						6.57 (8.8)						2.63 (5.2)					4.48 (5.9)		
	m2			12.58 (22.5)						8.82 (18.0)						2.87 (4.9)					2.35 (4.5)		
	m3			8.88 (12.7)						6.18 (12.6)						2.42 (4.2)					4.72 (7.9)		
	m4			11.17 (15.4)						7.85 (16.1)						3.60 (8.1)					1.72 (4.2)		
	m5			11.28 (16.8)						9.98 (20.4)						4.42 (8.6)					1.52 (2.4)		
	m6			10.53 (16.8)						7.37 (13.7)						2.72 (4.2)					2.05 (4.7)		
⟨2*ab*⟩	m1	−2.7	−4.0	17.0	−21.6	13.3	−2.5	3.2	−21.1	9.7	−3.2	−3.2	−4.9	−52.1	53.0	−54.7	56.4	−59.0	56.2	−58.8	67.7	91.3	−86.3
	m2	10.0	−9.2	14.1	−16.9	15.6	−13.7	3.1	−14.1	10.9	−5.2	5.3	−16.8	−55.2	51.8	−50.4	53.1	−60.1	60.5	−67.4	58.8	88.8	−88.0
	m3	1.8	−6.9	17.9	−21.7	14.6	−6.2	3.5	−22.0	10.3	−3.6	1.1	−7.7	−52.3	52.7	−54.4	56.2	−59.4	56.8	−57.6	68.8	89.7	−87.6
	m4	8.0	−9.6	16.1	−18.3	14.6	−11.1	3.4	−18.2	10.6	−4.6	4.5	−13.1	−54.2	52.3	−52.5	54.9	−60.3	59.4	−64.8	61.4	91.7	−84.2
	m5	6.2	−7.0	13.5	−16.8	14.1	−10.2	2.7	−14.9	9.3	−4.5	1.7	−14.2	−55.1	52.1	−50.7	53.1	−59.6	59.9	−67.8	58.5	88.1	−89.3
	m6	5.2	−7.8	15.7	−18.6	13.9	−8.7	3.5	−19.1	8.9	−4.0	2.4	−11.0	−53.6	51.8	−51.9	54.6	−60.2	59.0	−62.0	64.5	87.9	−89.2
Δ_{av}	m1			1.88 (3.4)						2.68 (4.4)						1.03 (2.1)					1.50 (2.4)		
	m2			1.95 (3.7)						2.05 (3.5)						0.52 (1.5)					0.7 (1.2)		
	m3			1.58 (3.3)						3.68 (11.4)						0.65 (1.3)					1.30 (2.2)		
	m4			1.33 (2.0)						2.02 (6.3)						1.57 (3.7)					1.90 (2.4)		
	m5			1.80 (2.9)						4.27 (13.9)						2.60 (4.9)					1.25 (2.0)		
	m6			1.17 (2.2)						3.12 (7.3)						1.13 (2.2)					0.80 (1.7)		
(2*A*) c(L-Pip-L-(NMe)Phe)																							
SM		11.9	−5.8	−8.2	16.2	−9.8	−3.8	−2.6	1.7	−12.1	0.5	6.7	−1.4	−54.2	53.2	−53.1	53.5	−57.1	57.5	67.5	−63.9	92.9	−87.0
Δ_{av}	m1			4.65 (8.2)						4.53 (11.6)						1.18 (2.1)					2.40 (3.6)		
	m2			5.70 (9.4)						5.63 (11.5)						1.07 (2.5)					1.60 (2.3)		
⟨2*ab*⟩	m1	18.1	−3.8	−18.0	25.6	−10.7	−10.3	−4.0	14.1	−17.9	−0.5	12.6	−7.6	−53.7	52.7	−53.9	55.5	−58.7	58.0	67.9	−60.7	89.5	−90.0
	m2	20.0	−5.2	−17.3	25.5	−10.3	−11.7	−3.9	14.6	−16.2	−0.8	13.3	−9.3	−54.7	53.0	−53.5	54.5	−59.1	59.5	67.3	−61.9	90.3	−90.4
Δ_{av}	m1			1.28 (2.2)						0.92 (2.2)						0.30 (0.7)					0.70 (1.2)		
	m2			1.15 (1.9)						0.85 (1.4)						0.38 (0.6)					1.50 (2.1)		
(2*B*) c(D-Pip-L-(NMe)Phe)																							
SM		18.4	−8.7	−12.4	24.1	−14.0	−6.6	−2.2	7.9	−14.7	1.4	15.2	0.6	52.7	−54.8	54.7	−53.7	54.7	−53.3	66.8	−62.6	91.9	−87.2
Δ_{av}				2.07 (3.6)						2.30 (6.8)						1.37 (1.8)					1.78 (3.0)		
⟨2*ab*⟩		16.3	−10.4	−10.8	25.9	−19.5	−0.9	−2.1	10.2	−9.3	2.4	13.0	8.8	53.2	−56.0	55.9	−54.1	54.2	−52.9	67.1	−60.5	90.0	−85.9
Δ_{av}				1.13 (2.3)						0.97 (2.4)						0.97 (2.0)					0.68 (0.9)		

essentially yield accurate geometries for the gas phase, the difference with the experimental X-ray structures reveals the effects of crystal packing. This makes it possible to interpret some of these differences in terms of the structural factors controlling the DKP conformation.

In the *non-methylated* compounds (1*A*), (1*B*) and (9*A*) intermolecular hydrogen bonds and other crystal packing forces apparently influence the DKP conformation to a great extent: elimination of all these interactions causes very substantial structural changes, particularly in the DKP rings. The crystal lattices of the pipecolic acid analogs (1*A*) and (1*B*) host multiple conformers with highly distorted peptide bonds. When used as starting geometries, each of these different structures collapses to one single conformation (taken up in Tables 3 and 4) in SM calculations. By contrast, the non-methylated proline analogs (9*A*) and (9*B*) have only one conformer in the asymmetric unit ($Z' = 1$) and maintain nearly planar peptide bonds in a $_{C\alpha}B$ boat form. The peculiar conformation of (9*A*) – which is needed in the crystal to enforce the tight packing of the hydrogen-bond chains –

Table 4
Torsion angles of the DKP ring, Pro ring and Phe side-chain and peptide bond (non)planarity parameters (in °) for (9*A*)–(10*B*) as obtained by single molecule (SM) and periodic (⟨2*ab*⟩) DFT calculations.

Δ_{av} is the average deviation between calculated and experimental X-ray angles inside each group and Δ_{max} is the largest group difference (values in parentheses).

	DKP ring						Peptide bond nonplanarity						Proline ring					Phe			
Method	ϕ_1	ψ_1	ω_1	ϕ_2	ψ_2	ω_2	χ(C5)	χ(N4)	τ(1)	χ(C2)	χ(N1)	τ(2)	$\chi1$	$\chi2$	$\chi3$	$\chi4$	$\chi5$	χ (α1)	χ (α2)	χ (β1)	χ (β2)
(9*A*) c(L-Pro-L-Phe)																					
SM	−31.6	27.5	5.6	−35.8	31.1	0.9	−1.2	−13.2	−0.8	−0.5	3.7	6.0	−34.3	36.7	−24.6	2.7	20.1	−62.4	174.4	101.3	−77.9
Δ_{av}	12.80 (19.2)						7.17 (21.8)						7.52 (11.9)					17.00 (17.9)			
⟨2*ab*⟩	−40.9	46.5	−3.7	−45.5	50.6	−8.2	0.7	8.7	0.6	−0.5	15.1	−0.7	−23.2	35.5	−33.7	20.0	2.0	−82.2	154.3	117.9	−61.5
Δ_{av}	2.45 (4.1)						3.78 (12.4)						4.12 (6.5)					1.18 (2.2)			
(9*B*) c(L-Pro-D-Phe)																					
SM	−26.9	23.9	−0.1	−22.6	20.1	3.9	−1.5	−2.1	−0.8	0.2	2.5	10.1	−36.6	35.1	−19.7	−3.9	25.9	−65.0	63.3	89.9	−89.0
Δ_{av}	5.67 (10.6)						3.03 (4.9)						2.94 (4.7)					10.90 (14.3)			
⟨2*ab*⟩	−14.7	13.1	4.3	−20.2	17.9	−1.4	0.6	0.3	8.2	0.1	12.2	9.3	−37.5	32.4	−14.7	−9.8	30.1	−75.7	52.0	83.9	−93.1
Δ_{av}	2.72 (4.0)						3.38 (7.1)						1.40 (2.2)					2.88 (3.3)			
(10*A*) c(L-Pro-L-(NMe)Phe)																					
SM	−1.3	8.6	−14.9	12.9	−4.4	−0.6	−6.0	3.6	−20.2	3.0	17.8	13.6	−39.4	31.8	−12.3	−13.5	33.9	67.6	−61.4	94.9	−84.8
Δ_{av}	5.97 (10.6)						3.43 (10.6)						7.12 (10.9)					3.45 (5.0)			
⟨2*ab*⟩	8.3	2.0	−18.0	23.3	−12.0	−2.7	−5.0	11.0	−20.0	3.1	25.3	16.8	−38.0	26.7	−5.2	−19.9	36.9	63.9	−64.2	90.0	−89.2
Δ_{av}	1.13 (2.2)						1.00 (3.2)						2.52 (3.8)					0.8 (1.6)			
(10*B*) c(L-Pro-D-(NMe)Phe)																					
SM	−30.9	27.2	−0.3	−25.0	22.1	5.5	−1.3	0.2	0.9	0.4	0.0	10.6	−36.3	35.8	−21.1	−2.3	24.6	−67.1	63.2	89.1	−90.0
Δ_{av}	2.97 (4.1)						2.43 (4.9)						2.52 (3.8)					1.30 (2.8)			
⟨2*ab*⟩	−28.6	26.3	1.8	−28.9	26.7	1.3	−1.0	−5.2	−0.6	0.7	4.9	6.9	−36.1	37.9	−24.6	1.6	22.0	−67.9	61.4	87.1	−91.1
Δ_{av}	0.47 (0.7)						0.52 (1.2)						1.58 (2.3)					0.62 (1.0)			

Table 5
Overview of MP2-energy differences (in kJ mol^{-1}) between the benzyl side-chain rotamers in (9*A*) and (9*B*) calculated using the single molecule (SM) and the hydrogen-bond (HB) approach.

Phe ring rotamer	SM		HB	
	(9*A*)	(9*B*)	(9*A*)	(9*B*)
F	0.17	0.00	5.53	0.00
E_N	0.00	9.34	0.00	13.65
E_O	7.87	18.25	3.52	32.03

changes considerably in the gas phase. In the non-methylated compound (9*B*), intermolecular interactions are much less determining the conformation. This structure is free of internal strain and therefore intrinsically stable.

For the *N-methylated* analogs (2*A*), (2*B*) and (10*A*), (10*B*) the SM simulations also closely reproduce the X-ray molecular structure, with average deviations Δ_{av} of the torsion angles < 5° for the *cis* isomers (2*A*) and (10*A*), and < 3° for the *trans* isomers (2*B*) and (10*B*). Amide bond non-planarity parameters observed in the crystals of (2*B*), (10*A*) and (10*B*) are very close (Δ_{av} of 2.3, 3.2 and 2.4°) to the SM results, while for (2*A*) Δ_{av} = 5°. The remarkable match down into the details between the SM and X-ray molecular shapes, including the sensitive non-planarity parameters of highly distorted amide bonds, is possible only if packing effects are negligible. Apparently in *N*-methyl analogs, in the absence of hydrogen bonds, the weaker and less directional packing forces act rather evenly in the three dimensions and exert little effect on the molecule's intrinsic conformational preference. Hence, their solid-state conformation is mostly controlled by the steric interaction between the *N*-methyl and the benzyl substituents, and by the fusion to the piperidine and pyrrolidine rings. The presence of a less-strained piperidine ring in (2*A*) and (2*B*) leads to larger deviations between the SM and crystal conformations, because the DKP ring is more flexible.

One intriguing issue in the chosen set of eight compounds is the orientation of the phenyl substituent. In all but one of the crystallographic structures, this group assumes a folded (*F*) conformation (see Fig. 3 for nomenclature). In (9*A*), however, the phenyl ring maintains an extended to nitrogen (E_N) conformation. To examine the energetic origin of this discrepancy, SM and HB geometry optimizations were performed using the MP2 method on all rotational conformers of the benzyl substituent in (9*A*) and (9*B*) (Table 5). The introduction of hydrogen bonds in the latter approach should give an indication of the effect of crystal packing on the preferential orientation. The optimized HB structures are given in the supplementary material.

Both the SM and HB approach indicate that the folded conformer is most stable for (9*B*), with an energy order $E_O > E_N > F$ that is even more pronounced when the crystal environment is taken into account. In (9*A*) a different pattern emerges: $E_O > F > E_N$. In the SM calculation, the extended to nitrogen conformer is marginally more stable than the folded one. Clearly, the *pseudo-equatorial* position of the benzyl group in the *F* rotamer does not give rise to favorable stacking of the phenyl group over the DKP ring. In the HB scheme, the ordering of the rotamers is $F > E_O > E_N$ maintaining but considerably increasing the energetic preference for the E_N rotamer. So these calculations confirm that the specific characteristics of its crystal lattice contribute to the E_N preference

in (9*A*). The packing efficiency of the (9*A*)'s E_N conformer (density D = 1.345 g cm^{-3}) is higher than those of the folded rotamers of (1*A*), (1*B*) and (9*B*) (D = 1.269, 1.235 and 1.308 g cm^{-3}), and presumably also better than that of (9*A*)'s folded rotamer.

3.4. Periodic calculations

Starting from the unit-cell structures obtained from the X-ray diffraction, geometry optimizations were performed within the periodic approach for all compounds. The results of these calculations are given in Table 3 and 4. It is clear that the periodic calculations reproduce the crystal geometries very well, validating the use of DFT to describe the peculiar structural aspects in these biomolecular crystals. This is most easily seen by considering the average (Δ_{av}) and maximum (Δ_{max}) difference between the calculations and the X-ray data, calculated separately for the DKP ring, peptide bond planarity, Pro/Pip ring and Phe substituent. The average deviation is always lower than 5° for all compounds, but in (1*A*), (1*B*) and (9*A*) the Δ_{max} value attains 10° or more due to χ(N1) or χ(N4). In (9*A*) this deviation is associated with an increased deformation of the fused proline ring, as attested by the χ5 value. In (1*A*), respectively and (1*B*) it is due to a difference in conformation of the N4—H bond in the m4, respectively the m3 and m5 DKP molecules of the unit cell. The divergence between theory and experiment on this point possibly indicates minor errors in the X-ray positions of the amide H atoms: *e.g.* in (1*B*) the N4—H distance can become unrealistically small (0.72 Å). Yet, it has to be stressed that the Dunitz parameters, describing the peptide bond non-planarity are very sensitive to even minute changes in geometry. For instance, although (9*A*) gives rise to a maximal deviation of 12.6°, the RMSD for the entire periodic cell is only 0.18 Å. Therefore, the overall attained accuracy of the periodic DFT calculations is very good.

The molecules in the optimized supercells of (1*A*), (1*B*) and (2*A*) also assume different conformations, in line with the X-ray observations. Even when all the molecules in the simulation cell are artificially altered to be identical, optimization destroys this equality. In some cases, alternative local minima are found after severe distortion of the DKP rings of the molecules in the cell and reoptimization. The resulting structures differ from those reported in Table 2, but the total energy of the entire simulation cell is higher (of the order of 4.2 kJ mol^{-1}). The existence of these local minima corroborates that the DKPs reside in a fairly broad minimum of the potential energy surface, where each molecule in the cell can assume slightly different conformations.

3.5. High Z' structures

As mentioned, the asymmetric parts of the unit cells of (1*A*), (1*B*) and (2*A*) contain symmetrically independent molecules, offering the opportunity to study differences in their molecular conformations. These structures mainly mutually differ in the conformation of the DKP ring, as can be seen in Table 2. The periodic calculations remain in general close to the multiple conformers of the crystal structures, but also indicate that minor structural distortions are easily possible. The SM calculations starting from each of the individual multiple conformers converge to one conformation that differs largely from all the original crystal conformers.

We consider the following as cumulative conditions to increase the likelihood of multiple conformers ($Z' > 1$) in the crystal structures:

(i) *The single molecule should possess an inherent flexibility*: The Cα boat of the proline-fused DKPs resides in a relatively deep and narrow energy minimum, while ring fusion to the six-membered piperidine ring in Pip analogs flattens the DKP ring in a broad and shallow energy valley in which the DKP ring can be deformed at low energy cost to different conformations that are virtually degenerate. Note that the amide bond's easy deviation from planarity and its pivotal position in the center of the molecule are mainly responsible for the overall molecular flexibility.

(ii) *A strongly directional and closely packed submotif*: In (1*A*) and (1*B*) hydrogen-bond networking forms closely packed one-dimensional motifs (hydrogen-bond chains) along their crystallographic *a* and *b* axes. In both cases packing in the remaining dimensions relies *only* on less directional and weaker non-classical C—H···O hydrogen bonds, van der Waals and dispersive forces.

If the shapes of the relatively rigid one-directional packing motifs do not pack efficiently *and* if the single molecules in the motif have flexible torsions, different conformations can lead to new packing modes, trading intramolecular with intermolecular energy.

4. Conclusion

This paper reports and compares a consistent series of eight new crystal structures of *cis* and *trans* cyclic dipeptides of Phe or (NMe)Phe and Pip or Pro at the same temperature (150 K). In general, the observed impact of the three embodied structural differences (*N*-methylation, side-chain ring size and *cis*/*trans* configuration) on the molecular structures is in line with DFT single molecule calculations and with established conformational aspects of cyclic dipeptides. Advanced computer simulations of the molecules in the isolated states as well as in the crystal environment allowed to separate (to a certain level) the inter- and intramolecular factors and revealed part of the interplay between them. Thus, the exceptional high pucker of the DKP ring in the crystal structure of *cyclo*(L-Pro-L-Phe) (9*A*) can be attributed to the combined action of strong hydrogen-bond and C═O/C═O dipole packing forces.

In the non-methylated analogs (1*A*), (1*B*), (9*A*), (9*B*) crystal packing is dominated by strong and directional hydrogen bonds that result in one-dimensional chain motifs. The *N*-methylated analogs, depending on the space group, either segregate in double layers [(2*A*), (10*A*)] or form a more isotropic three-dimensional-network [(2*B*), (10*B*)].

The effects of side-chain ring size and the change from *cis* to *trans* configuration are more subtle. Relatively small differ-

ences in molecular structure can have a large impact on the arrangement of molecules in the crystalline state. Compounds (1*A*) and (1*B*) that have a relatively flat and flexible DKP ring fused with the rigid six-membered piperidine ring show multiple conformers in their hydrogen-bond chain motifs. This illustrates that the crystal packing can considerably affect the conformation of flexible molecules. The proline analogs (9*A*) and (9*B*), with the DKP ring fused to a five-membered pyrrolidine ring, crystallize as a single structure with a considerably puckered boat conformation of the central DKP ring, that is either intrinsically stable and rigid (9*B*) or strongly stabilized by packing forces (9*A*).

As computational technology develops further and additional crystal structures appear, our understanding of the packing of organic molecules will improve. Cyclic dipeptides will continue to play a central role as model compounds in this process. This work provides a frame of reference for future studies that aim at the evaluation of the effect of substitution of a CH_2 group by a sulfur atom in the cyclic side-chains.

The authors are grateful to Professor M. Anteunis who initiated this project. Furthermore, the authors thank the FWO (Fonds voor Wetenschappelijk Onderzoek, Vlaanderen, Fund for Scientific Research, Flanders), the research board of the Ghent University and the IAP-BELSPO project in the frame of IAP 6/27 for financial support of this research. Computational resources and services used in this work were provided by Ghent University and IOCB Prague. One of the authors (MB) thanks to Grant Agency of the Czech Republic for financial support of his working visits in Ghent University (grant 203/09/1919). IC thanks to MSM0021620857.

References

Altomare, A., Cascarano, G., Giacovazzo, C., Guagliardi, A., Burla, M. C., Polidori, G. & Camalli, M. (1994). *J. Appl. Cryst.* **27**, 435.
Anteunis, M. J. O. (1978). *Bull. Soc. Chim. Belg.* **87**, 627–650.
Anteunis, M. J. O., Schroten, R., Nachtergaele, W. & Neirinckx, I. (1979). *Bull. Soc. Chim. Belg.* **88**, 683–694.
Becke, A. D. (1992). *J. Chem. Phys.* **96**, 2155–2160.
Becke, A. D. (1996). *J. Chem. Phys.* **104**, 1040–1046.
Bouř, P., Sychrovský, V., Maloň, P., Hanzlíková, J., Baumruk, V., Pospíšek, J. & Budesinsky, M. (2002). *J. Phys. Chem. A*, **106**, 7321–7327.
Budesinsky, M., Symersky, J., Jecny, J., Van Hecke, J., Hosten, N., Anteunis, M. J. O. & Borremans, F. (1992). *Int. J. Pept. Protein Res.* **39**, 123–130.
Cascarano, G., Altomare, A., Giacovazzo, C., Guagliardi, A., Moliterni, A. G. G., Siliqi, D., Burla, M. C., Polidori, G. & Camalli, M. (1996). *Acta Cryst.* A**52**, C79.
Chin, D. N., Palmore, G. T. R. & Whitesides, G. M. (1999). *J. Am. Chem. Soc.* **121**, 2115–2122.
Cotrait, M. & Leroy, F. (1979). *Cryst. Struct. Commun.* **8**, 819–822.
CPMD (1990–2006). CPMD V3.11 Copyright IBM Corp. Copyright MPI fur Festkoerperforschung Stuttgart 1997–2001.
Desiraju, G. R. (1995). *Angew. Chem. Int. Ed.* **34**, 2311–2327.
Dunning, T. H. Jr (1989). *J. Chem. Phys.* **90**, 1007–1023.
Enraf–Nonius (1994). *CAD*4 *EXPRESS*, Version 5.1/1.2. Enraf–Nonius, Delft, The Netherlands.
Flack, H. D. (1983). *Acta Cryst.* A**39**, 876–881.
Fischer, P. M. (2003). *J. Pept. Sci.* **9**, 9–35.
Frisch, M. J. *et al.* (2004). *GAUSSIAN03*, Revision B.04. Gaussian, Inc., Wallingford CT, USA.
Gdaniec, M., Liberek, B., Kolodziejczyk, A. S., Jankowska, R. & Ciarkowski, R. (1987). *Int. J. Pept. Protein Res.* **30**, 79–92.
Hao, X., Chen, J., Cammers, A., Parkin, S. & Brock, C. P. (2005). *Acta Cryst.* B**61**, 218–226.
Hendea, D., Lachat, S., Baro, A. & Frey, W. (2006). *Helv. Chim. Acta*, **89**, 1894–1909.
Hooft, R. W. W. (1998). *COLLECT*. Enraf–Nonius, Delft, The Netherlands.
Jankowska, R. & Ciarkowski, J. (1987). *Int. J. Pept. Protein Res.* **30**, 61–78.
Karle, I. L. (1972). *J. Am. Chem. Soc.* **94**, 81–84.
Koch, W. & Holthausen, M. C. (2001). *A Chemist's Guide to Density Functional Theory*, 2nd ed. Weinheim: Wiley-VCH.
Krishnan, R., Binkley, J. S., Seeger, R. & Pople, J. A. (1980). *J. Chem. Phys.* **72**, 650–654.
Leeuw, F. A. A. M. de, Altona, C., Kessler, H., Bermel, W., Friedrich, A., Krack, G. & Hulll, W. E. (1983). *J. Am. Chem. Soc.* **105**, 2237–2246.
Lenstra, A. T. H., Verbruggen, M., Bracke, B., Vanhouteghem, F., Reyniers, F. & Borremans, F. (1991). *Acta Cryst.* B**47**, 92–97.
MacDonald, J. C. & Whitesides, G. M. (1994). *Chem. Rev.* **94**, 2383–2420.
Mazza, F., Lucente, G., Pinnen, F. & Zanotti, G. (1984). *Acta Cryst.* C**40**, 1974–1976.
McKinnon, J. J., Jayatilaka, D. & Spackman, M. A. (2007). *Chem. Commun.* **37**, 3814–3816.
Meetsma, A. (2006). Personal communication.
Otwinowski, Z. & Minor, W. (1997). *Methods Enzymol.* **276**, 307–326.
Palacin, S., Chin, D. N., Simanek, E. E., MacDonald, J. C., Whitesides, G. M., McBride, M. T. & Palmore, G. T. R. (1997). *J. Am. Chem. Soc.* **119**, 11807–11816.
Pauwels, E., Van Speybroeck, V. & Waroquier, M. (2004). *J. Phys. Chem. A*, **108**, 11321–11332.
Perdew, J. P. (1986). *Phys. Rev. B*, **33**, 8822–8824.
Petricek, V., Dusek, M. & Palatinus, L. (2006). *JANA*2006. Institute of Physics, Praha, Czech Republic.
Rajappa, S. & Natekar, M. V. (1993). *Advances in Heterocyclic Chemistry*, pp. 187–289. San Diego: Academic Press.
Ramani, R., Venkatesan, K., Marsh, R. E. & Hu Kung, W.-J. (1976). *Acta Cryst.* B**32**, 1051–1056.
Sammers, P. G. (1975). *Fortschritte der Chemie Organischer Naturstoffe*, pp. 51–118. Vienna: Springer-Verlag.
Sheldrick, G. M. (2008). *Acta Cryst.* A**64**, 112–122.
Spackman, M. A. & McKinnon, J. J. (2002). *CrystEngComm*, **4**, 378–392.
Symerský, J., Huml, K. & Petříček, V. (1987). *Acta Cryst.* C**43**, 1603–1607.
Tsuzuki, S., Honda, K., Uchimaru, T., Mikami, M. & Fujii, A. (2006). *J. Phys. Chem. A*, **110**, 10163–10168.
Vanderbilt, D. (1990). *Phys. Rev. B*, **41**, 7892–7895.
Van Poucke, M., Geize, H. J. & Lenstra, A. T. H. (1982). *Bull. Soc. Chim. Belg.* **91**, 213–218.
Vicar, J., Budesinsky, M. & Blaha, K. (1973). *Collect. Czech. Chem. Commun.* **38**, 1940–1946.
Winkler, F. K. & Dunitz, J. D. (1971). *J. Mol. Biol.* **59**, 169–182.
Zhu, Y., Tang, M., Shi, X. & Zhao, Y. (2006). *Int. J. Quantum Chem.* **107**, 745–753.